International Journal of Heat and Mass Transfer 77 (2014) 627–652

Contents lists available at ScienceDirect

International Journal of Heat and Mass Transfer

journal homepage: www.elsevier.com/locate/ijhmt

Review

Review of databases and predictive methods for heat transfer in condensing and boiling mini/micro-channel flows

Sung-Min Kim, Issam Mudawar *

Purdue University Boiling and Two-Phase Flow Laboratory (PU-BTPFL), Mechanical Engineering Building, 585 Purdue Mall, West Lafayette, IN 47907-2088, USA

ARTICLE INFO

Article history:
Received 10 May 2014
Received in revised form 18 May 2014
Accepted 19 May 2014
Available online 23 June 2014

Keywords:
Heat transfer
Dryout incipience
Flow boiling
Condensation
Mini-channel
Micro-channel

ABSTRACT

The importance of flow boiling and condensing mini/micro-channel devices to a large number of modern applications has spurred an unusually large number of research efforts that culminated in many types of predictive tools. These efforts have inadvertently contributed enormous confusion when selecting a suitable predictive method. This study reviews methods for predicting heat transfer in condensing and boiling mini/micro-channel flows. Systematic assessment of predictive accuracy of individual methods requires the development of consolidated mini/micro-channel databases for condensation heat transfer, dryout incipience quality, and saturated boiling heat transfer. These databases cover numerous working fluids and broad ranges of geometrical and flow parameters. It is shown that, despite the success of previous predictive methods for specific fluids and narrow databases, these methods are incapable of providing accurate predictions against entire consolidated databases. The consolidated databases are used to develop 'universal' correlations with very broad application range. These include two separate correlations for condensation heat transfer, one for annular flow and the other for slug and bubbly flows. Also developed are correlations for dryout incipience quality and saturated boiling heat transfer; the later is shown to accurately tackle both nucleate boiling dominated and convective boiling dominated regimes up to the location of incipient dryout.

Contents

* Corresponding author. Tel.: +1 (765) 494 5705; fax: +1 (765) 494 0539.
E-mail address: mudawar@ecn.purdue.edu (I. Mudawar).
URL: https://engineering.purdue.edu/BTPFL (I. Mudawar).

http://dx.doi.org/10.1016/j.ijheatmasstransfer.2014.05.036
0017-9310/

Nomenclature

A	flow area
Bd	Bond number, $Bd = g(\rho_f - \rho_g)D_h^2/\sigma$
Bo	Boiling number, $Bo = q''_H/(Gh_{fg})$
c_p	specific heat at constant pressure
C	parameter in Lockhart–Martinelli correlation
C_1, C_2	empirical coefficients
Ca	capillary number, $Ca = (\mu_f G)/(\rho_f \sigma)$
Co	convection number, $Co = ((1-x)/x)^{0.8}(\rho_g/\rho_f)^{0.5}$
D	tube diameter
D_h	hydraulic diameter
e	surface roughness
E	empirical coefficient
f	Fanning friction factor; function
F	empirical coefficient
Fr	Froude number
Fr^*	modified Froude number
g	gravitational acceleration
G	mass velocity
h	heat transfer coefficient
h_{fg}	latent heat of vaporization
h_{tp}	two-phase heat transfer coefficient
H_{ch}	height of rectangular channel
k	thermal conductivity
L	channel length
M	molecular weight
N	number of data points; number of channels; empirical coefficient
N_{conf}	confinement number, $N_{conf} = \sqrt{\sigma/(g(\rho_f - \rho_g)D_h^2)}$
Nu	Nusselt number
p	pressure
p_{crit}	critical pressure
P_F	wetted perimeter of channel
P_H	heated perimeter of channel
P_R	reduced pressure, $P_R = p/p_{crit}$
Pr	Prandtl number
Pr_T	turbulent Prandtl number
q''	heat flux
q''_{base}	heat flux averaged over base of heat sink
q''_H	effective heat flux averaged over heated/cooled perimeter of channel
Re	Reynolds number
Re_{eq}	equivalent Reynolds number
Re_f	superficial liquid Reynolds number, $Re_f = G(1-x)D_h/\mu_f$
Re_{fo}	liquid-only Reynolds number, $Re_{fo} = GD_h/\mu_f$
Re_g	superficial vapor Reynolds number, $Re_g = GxD_h/\mu_g$
Re_{go}	vapor-only Reynolds number, $Re_{go} = GD_h/\mu_g$
S	empirical coefficient
Su	Suratman number
T	temperature
$T_{w,std}$	standard deviation of wall temperature
T^+_δ	dimensionless boundary layer temperature
u^*	friction velocity
v	specific volume
W	width of heat sink
W_{ch}	width of channel
We	Weber number
We^*	modified Weber number
x	thermodynamic equilibrium quality
x_{crit}	dryout completion (CHF) quality
x_{di}	dryout incipience quality
Δx	quality change
X	Lockhart–Martinelli parameter, $X = \sqrt{(dp/dz)_f/(dp/dz)_g}$
X_{tt}	Lockhart–Martinelli parameter based on turbulent liquid-turbulent vapor flows
y	distance normal to the wall
y^+	dimensionless distance normal to the wall, $y^+ = yu^*/v_f$
z	stream-wise coordinate

Greek Symbols

β	channel aspect ratio ($\beta < 1$)
δ	thickness of condensing film
δ^+	dimensionless thickness of condensing film, $\delta^+ = \delta u^*/v_f$
ε_m	eddy momentum diffusivity
θ	percentage predicted within ±30%
μ	dynamic viscosity
v	kinematic viscosity
ξ	percentage predicted within ±50%
ρ	density
σ	surface tension
τ_w	wall shear stress
ϕ	two-phase multiplier

Subscripts

3	based on three-sided heat transfer in rectangular channel
4	based on four-sided heat transfer in rectangular channel
ann	annular flow
avg	average
cb	convective boiling dominant heat transfer
cir	based on uniform circumferential heating/cooling
crit	critical
exp	experimental (measured)
f	saturated liquid
fo	liquid only
g	saturated vapor
go	vapor only
in	inlet
k	liquid (*f*) or vapor (*g*)
nb	nucleate boiling dominant heat transfer
non-ann	slug and bubbly flow
pred	predicted
sat	saturation
sp	single-phase
tp	two-phase
tt	turbulent liquid–turbulent vapor
tv	turbulent liquid–laminar vapor
vt	laminar liquid–turbulent vapor
vv	laminar liquid–laminar vapor
w	wall

1. Introduction

The aggressive miniaturization of electronic components that commenced in the 1980s rapidly increased heat dissipation rate per unit device area. This increase spurred the development of innovative cooling schemes to maintain device temperatures below limits set by both materials and device reliability. Initial efforts focused on the use of fan-cooled heat sink attachments. But, given the poor thermophysical properties of air, interest quickly shifted to the use of dielectric liquids using single-phase cooling schemes. As heat dissipation from advanced computer devices exceeded 100 W/cm^2 by the mid-1980s [1], interest shifted

once again to two-phase cooling schemes. Unlike single-phase schemes, which rely entirely on the coolant's sensible heat rise, two-phase schemes capitalize on the coolant's combined sensible and latent heat to absorb far greater amounts of heat while maintaining relatively low device temperatures.

These cooling challenges were not limited to computer chips. By the early 1990s, similar challenges were being encountered in numerous medical, transportation, energy, aerospace, and defense applications [2]. Developments in these applications spurred intense research and development efforts aimed at incorporating

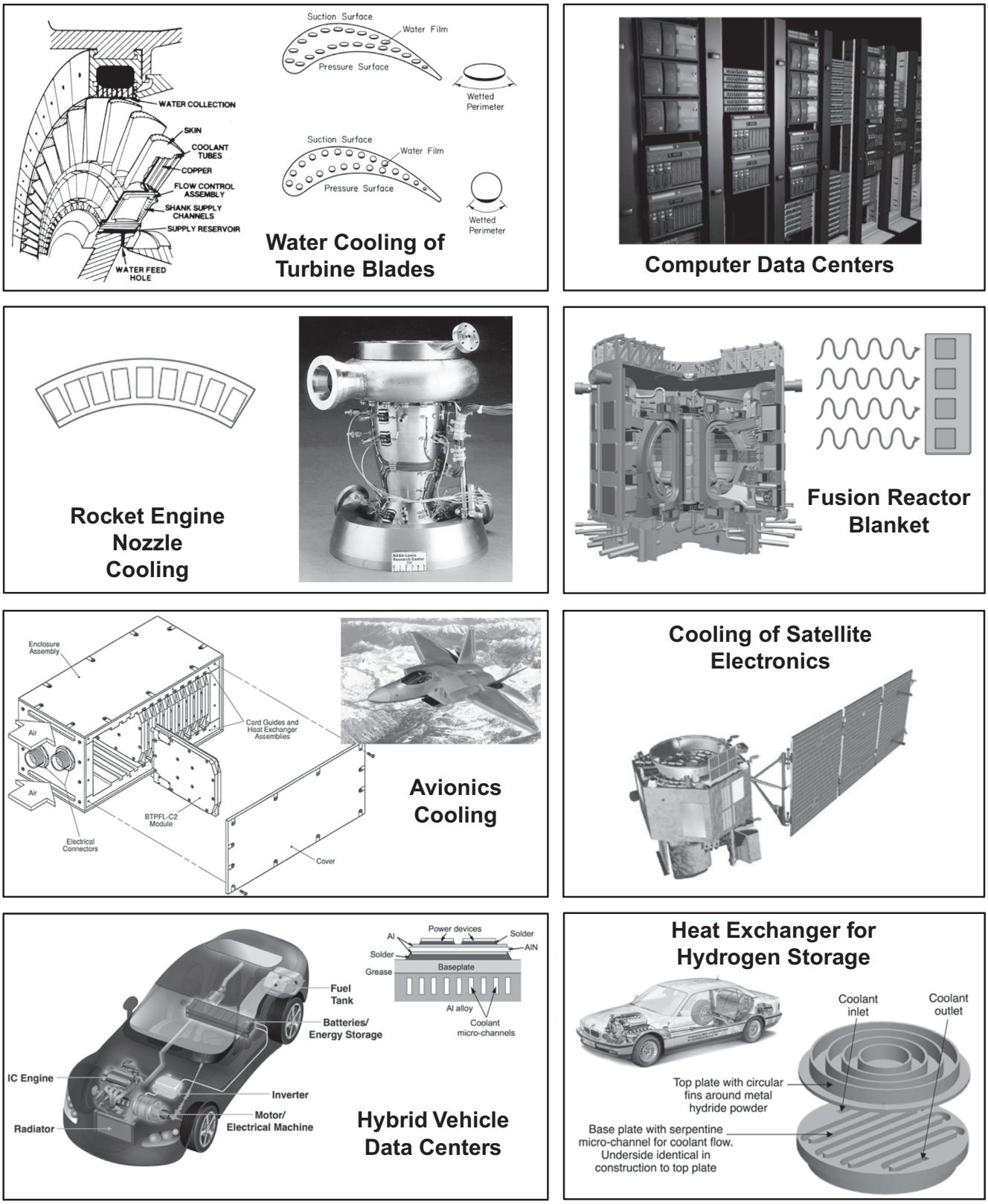

Fig. 1. Examples of applications of high-flux mini/micro-channel cooling.

high performance two-phase cooling solutions using a variety of cooling configurations and surface enhancement techniques [3–5]. Three cooling configurations have attracted the most attention: mini/micro-channel, jet and spray. Two-phase mini/micro-channel heat sinks are highly compact and lightweight, require very small coolant inventory, and provide very high heat transfer coefficients with good surface temperature uniformity [1,6,7]. Jet-impingement produces very high heat transfer coefficients in the jet stagnation zone [8]. This often results in larger surface temperature gradients, which can be circumvented by using multiple jets [9–11], requiring far greater coolant flow rates than mini-micro-channel heat sinks. There are also hybrid cooling schemes that combine the cooling merits of both mini/micro-channels and jets, producing both very high heat transfer coefficients and superior temperature uniformity [12,13]. Spray cooling offers the merits of high heat transfer coefficients and moderate surface temperature uniformity, but is generally more complicated to implement because of large packaging volume requirements and sensitivity of cooling performance to an unusually large number of spray parameters [14,15].

Given their relative cooling merits, ease of fabrication, and small coolant inventory, two-phase mini/micro-channel cooling devices have gained unprecedented popularity in many modern technologies demanding the removal of highly concentrated heat loads from small surface areas. These devices can also be implemented with both flow boiling and condensation. As shown in Fig. 1, two-phase mini/micro-channel flow has become increasingly important in many applications, including water cooled turbine blades [16], computer data centers [1,2], rocket nozzle cooling [17], fusion reactor blanket cooling [18,19], avionics cooling [20], cooling of satellite electronics [21], cooling of hybrid vehicle power electronics [22], and heat exchangers for hydrogen storage systems [23]. From a practical standpoint, mini/micro-channel cooling has shown great versatility in design and construction, including isolated tubes, tubes that are soldered upon a heat dissipating surface, and channels that are formed into a conducting substrate. There is also the added flexibility in mini/micro-channel shape, including circular [24], rectangular [25], triangular [26], trapezoidal [27,28] and diamond [29] cross sections, with hydraulic diameters in the range of 0.04–2.54 mm.

Despite their many cooling and practical packaging merits, two-phase mini/micro-channel devices are not without shortcomings, especially high pressure drop [30,31]. Flow boiling in small channels can also yield appreciable compressibility and flashing, or even two-phase choking [24]. There is also the likelihood of severe flow instabilities and oscillations in multi-channel heat sinks, which can induce premature critical heat flux (CHF) [32]. Heat transfer limits associated with CHF include departure from nucleate boiling (DNB), dryout, and premature CHF. And unlike single-phase flow in mini/micro-channels, which is highly predictable, using both popular correlations and computational methods [33], predicting two-phase flow in mini/micro-channel remains quite illusive.

Fig. 2(a) shows representative flow regimes associated with condensation of FC-72 in a micro-channel heat sink with multiple rectangular channels at different locations from the channel inlet [30]. A smooth-annular flow regime is initiated in the inlet region with the formation of a very thin liquid film along the channel walls. The condensation causes an axial increase in liquid flow rate, which is manifest in the wavy-annular regime by a thicker liquid film with appreciable interfacial waviness. Unlike flow boiling in mini/micro-channels, the interfacial waves in condensing flow do not appear to shatter or produce droplets in the central vapor core. As the film thickens farther downstream, wave crests in the transition regime begin to merge across the vapor care, triggering a transition to the slug flow regime. With further condensation, the oblong cylindrical bubbles gradually decrease in length, finally shrinking into spherical bubbles with a diameter close to the channel width. With a sufficiently long channel, all the vapor will eventually condense, resulting in pure liquid flow.

Fig. 2(b) shows representative flow regimes associated with flow boiling of FC-72 in a micro-channel heat sink with multiple rectangular channels at different operating conditions [34]. Bubbly flow is initiated by nucleation of discrete vapor bubbles along the channel walls near the channel inlet. Further evaporation increases vapor production by increasing both the size and number of bubbles. In the ensuing slug flow regime, the vapor bubbles coalesce into oblong bubbles with a diameter dictated by the channel width. Further evaporation triggers a transition to the churn flow regime, where the oblong vapor bubbles begin to break up, and the flow becomes chaotic and oscillatory. Eventually, an annular flow regime is formed as oblong vapor bubbles merge to form a continuous vapor core with a liquid film sheathing the channel walls.

Fig. 3(a) shows a schematic of axial variation of the heat transfer coefficient for condensation along a mini/micro-channel with a circumferentially uniform heat flux. The flow enters the channel as single-phase vapor, and is gradually converted to liquid due to condensation along the channel wall. The annular flow regime is

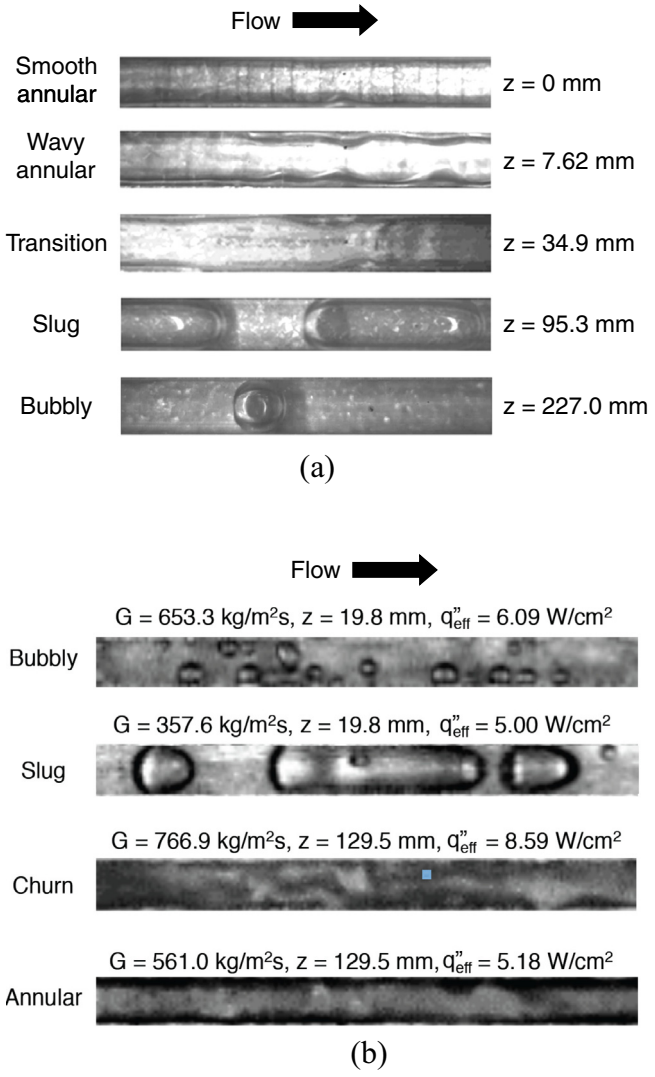

Fig. 2. Representative flow regimes for FC-72 in multi-channel heat sink containing rectangular channels for (a) condensation with D_h = 1.0 mm and G = 68 kg/m^2 s (adapted from [30]), and (b) flow boiling with D_h = 375.3 μm (adapted from [34]).

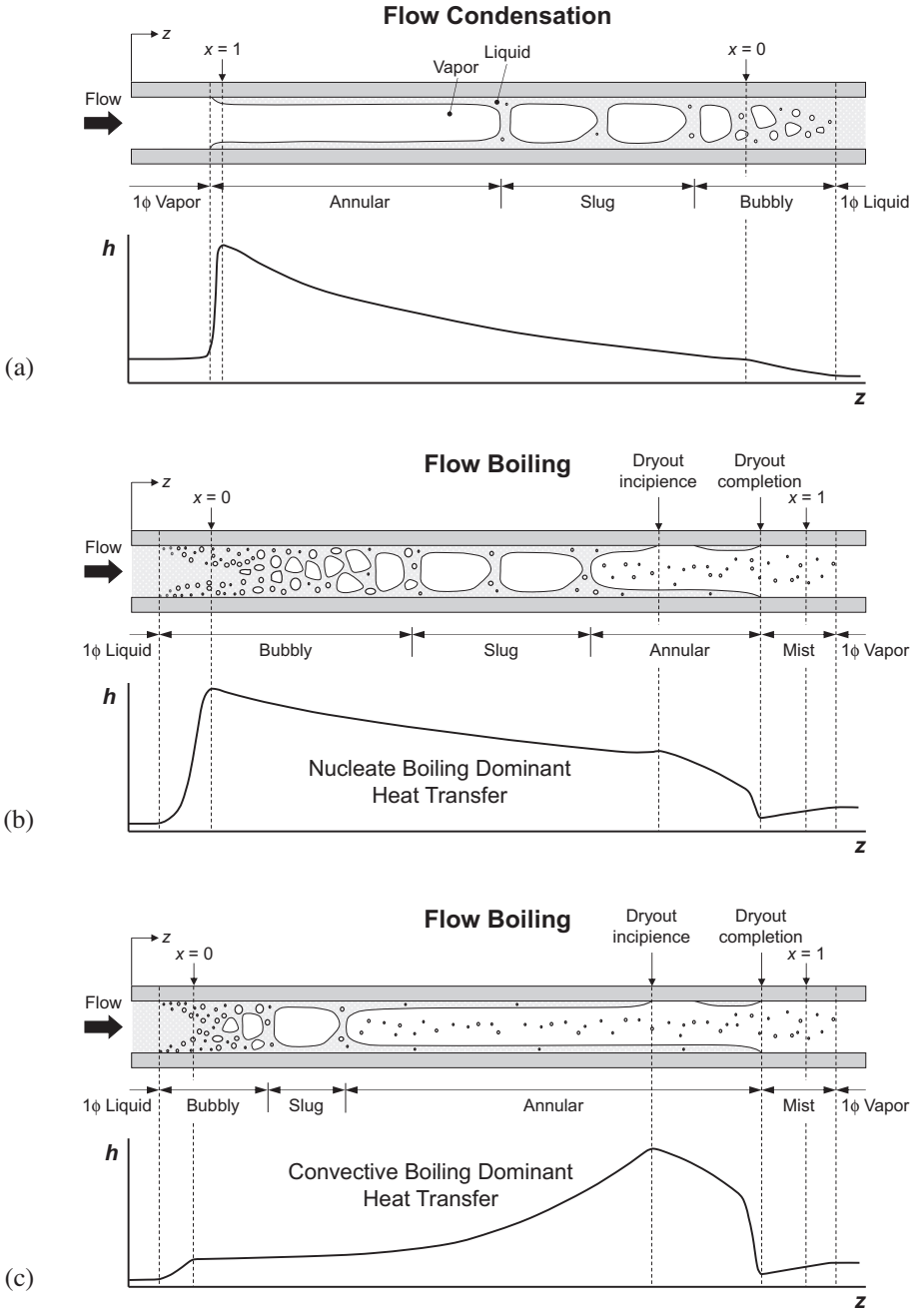

Fig. 3. Schematics of flow regimes, and variation of heat transfer coefficient in mini/microchannels with uniform circumferential heat flux for (a) condensation heat transfer, (b) nucleate boiling dominant heat transfer, and (c) convective boiling dominant heat transfer.

initiated in the upstream region of the channel with formation of a very thin liquid film. Heat transfer in this region is associated with a very small conduction resistance, resulting in very high heat transfer coefficients. Due to thermodynamic non-equilibrium effects, the condensation heat transfer coefficient is highest at a point slightly downstream of the onset of annular flow, where the thermodynamic equilibrium quality is equal to unity. Condensation along the channel causes gradual thickening of the liquid film and transition to the slug, bubbly and liquid flow regimes, and is associated with a gradual decrease in the heat transfer coefficient.

Fig. 3(b) and (c) show schematics of axial variations of the heat transfer coefficient for flow boiling along a mini/micro-channel corresponding to two distinct heat transfer regimes. These regimes are based on mechanisms that dominate the largest fraction of channel length upstream of the dryout location. Depicted in Fig. 3(b) is the *Nucleate Boiling Dominant* heat transfer regime, where the bubbly and slug flow regimes occupy a significant fraction of the channel length, and the heat transfer coefficient decreases monotonically along the channel due to gradual suppression of nucleate boiling. In contrast, Fig. 3(c) depicts the *Convective Boiling Dominant* heat transfer regime, where a significant fraction of the channel length is dominated by annular flow, and the heat transfer coefficient increases along the channel due to gradual thinning of the annular liquid film. For both heat transfer regimes, the heat transfer coefficient begins to decrease appreciably where dry patches begin to form at the location of *Dryout Incipience* (*i.e.*, onset of dryout, or partial dryout). *Dryout Completion*,

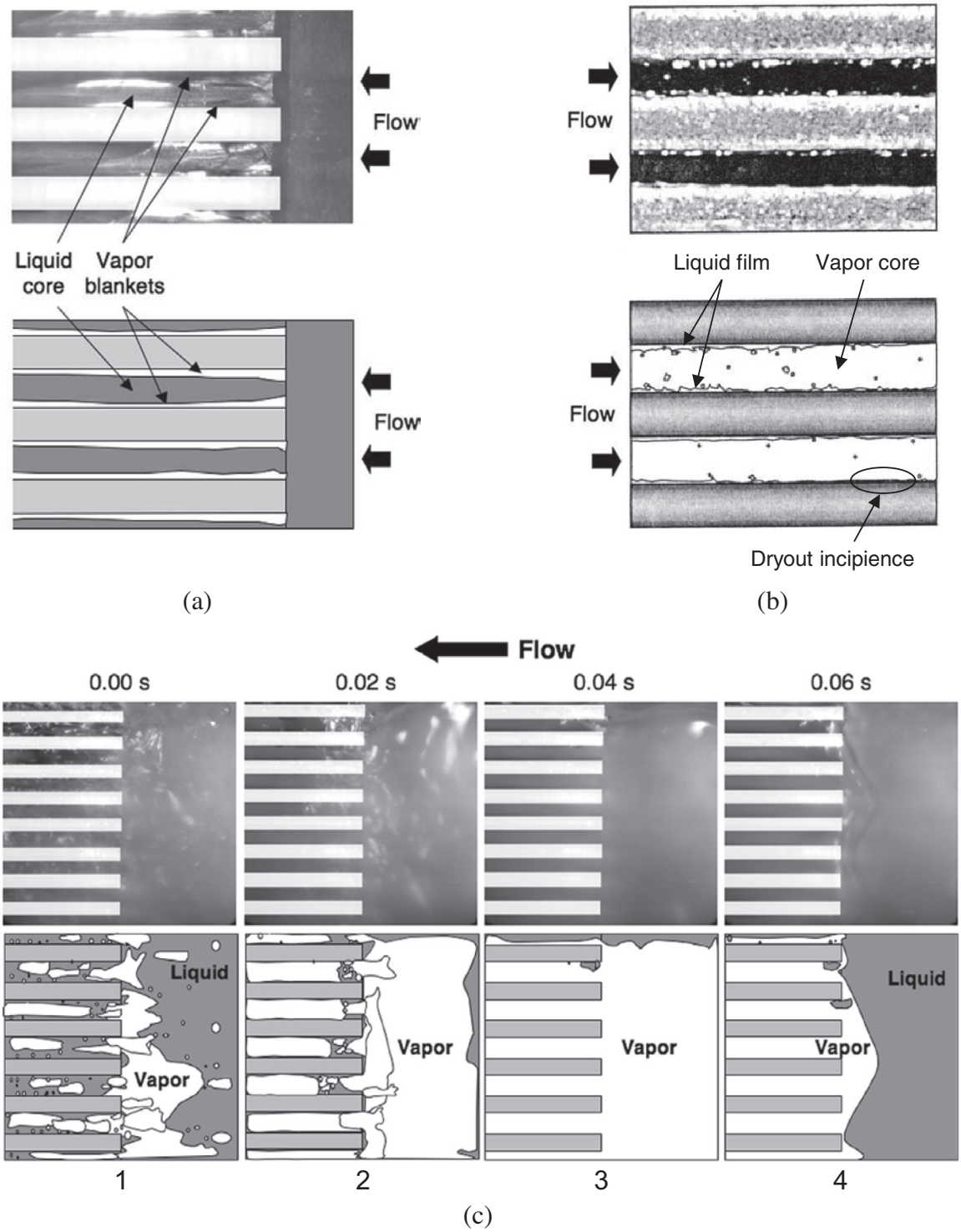

Fig. 4. CHF mechanisms in mini/micro-channel heat sinks. (a) DNB for HFE-7100 in heat sink with D_h = 334.1 μm for T_{in} = 0 °C, G = 1341 kg/m$_2$ s and q''_{base} = 325.8 W/cm^2 (adapted from [32]). (b) Dryout incipience for R134a in heat sink with D_h = 348.9 μm for x = 0.68, G = 128 kg/m^2 s and q''_{base} = 31.6 W/cm^2 (adapted from [97]). (c) Premature CHF and flow oscillations for HFE-7100 in heat sink with D_h = 415.9 μm for T_{in} = 0 °C, G = 670 kg/m^2 s and q''_{base} > 250.0 W/cm^2: (1) initial vapor pocket buildup in upstream plenum, (2) growth of vapor mass, (3) complete blockage of inlet plenum by vapor mass, and (4) purging of vapor mass along micro-channels (adapted from [32]).

which is commonly referred to as CHF, eventually occurs at a location farther downstream, where the liquid film is fully consumed.

Studies on two-phase flow in mini/micro-channels [31,35–112] have resulted in different approaches to predicting heat transfer. The vast majority of there studies are based on semi-empirical correlations for flow condensation heat transfer [58,60,113–122], dryout incipience quality [78,86,123–129], and flow boiling heat transfer [6,68,78,79,130–138]. But as the number of studies addressing these topics continues to rise, thermal design engineers are confronted with tremendous confusion in selecting a suitable correlation. This confusion can be traced to limitations of most published predictive methods to one or a few fluids and to

Table 1
Condensation heat transfer data for mini/micro-channel flows included in the consolidated database [142].

Author(s)	Channel geometry[a]	Channel material	D_h (mm)	Fluid(s)	G (kg/m^2 s)	Test mode	Data points
Dobson et al. [35]	C single, H	Copper	4.57	R134a, R12	75–653	Quasi-local h Δx = 0.1–0.2	76
Dobson et al. [36]	C single, H	Copper	4.57	R22	75–509	Quasi -local h Δx = 0.24 (avg)	32
Dobson et al. [37]	C single, H	Copper	3.14	R134a, R22	53–807	Quasi-local h Δx = 0.23 (avg)	165
Hirofumi and Webb [38]	C/R multi, H	Aluminum	0.96–2.13	R134a	200–1403	Quasi-local h Δx = 0.12 (avg)	62
Zhang [39]	C single/multi, H	Copper, aluminum	2.13, 3.25, 6.20	R134a, R22, R404A	200–1000	Quasi-local h Δx < 0.25	80
Wang [40]	R multi, H	Aluminum	1.46	R134a	79–761	Local h	748
Yan and Lin [41]	C multi, H	Copper	2.0	R134a	100–200	Quasi-local h small Δx	78
Baird et al. [42]	C single, H	Copper	1.95	R123	170–570	Local h	143
Kim et al. [43]	R multi, H	Aluminum	1.41	R410A, R22	200–600	Quasi-local h q'' = 0.5–1.5 W/cm^2	19
Jang and Hrnjak [44]	C single, H	Copper	6.10	CO_2	197–406	Quasi-local h small Δx	85
Cavallini et al. [45]	R multi, H	Aluminum	1.4	R410A, R134a	200–1400	Quasi-local h Δx = 0.2–0.3	59
Mitra [46]	C single, H	Copper	6.22	R410A	200–800	Quasi-local h Δx = 0.21 (avg)	144
Shin and Kim [47]	C/R single, H	Copper	0.493–1.067	R134a	100–600	Quasi-local h small Δx	237
Andresen [48]	C single/multi, H	Aluminum, copper	0.76, 1.52, 3.05	R410A	200–800	Quasi-local h Δx = 0.32 (avg)	315
Bandhauer et al. [49]	C multi, H	Aluminum	0.506, 0.761, 1.524	R134a	150–750	Quasi-local h small Δx	128
Agra and Teke [50]	C single, H	Copper	4.0	R600a	57–118	Quasi-local h small Δx	50
Kim et al. [51]	C single, H	Copper	3.48	CO_2	200–800	Quasi-local h small Δx	48
Marak [52]	C single, VU	Stainless steel	1.0	Methane	162–701	Quasi-local h Δx = 0.04 (avg)	129
Matkovic et al. [53]	C single, H	Copper	0.96	R134a, R32	100–1200	Local h	161
Park and Hrnjak [54]	C multi, H	Aluminum	0.89	CO_2	200–800	Quasi-local h Δx < 0.3	113
Agarwalet al. [55]	R multi, H	Aluminum	0.424, 0.762	R134a	150–750	Quasi-local h small Δx	43
Bortolin [56]	C/R single, H	Copper	0.96, 1.23	R245fa, R134a	67–789	Local h	309
Del Col et al. [57]	C single, H	Copper	0.96	R1234yf	200–1000	Local h	66
Huang et al. [58]	C single, H	Copper	1.6, 4.18	R410A	200–600	Quasi-local h Δx = 0.2	35
Oh and Son [59]	C single, H	Copper	1.77	R22, R134a, R410A	450–1050	Local h	108
Park et al. [60]	R multi, VD	Aluminum	1.45	R134a, R236fa, R1234ze (E)	100–260	Local h	204
Derby et al. [61]	R multi, H	Copper	1.0	R134a	75–450	Quasi-local h Δx < 0.3	140
Kim and Mudawar [31]	R multi, H	Copper	1.0	FC-72	118–367	Local h	268
Total							4045

[a] C: circular, R: rectangular, H: horizontal, VU: vertical upflow, VD: vertical downflow.

relatively narrow ranges of operating parameters. Eliminating this confusion represents a key objective of this study, following the same methodology adopted by the authors in a recent comprehensive review of pressure drop in condensing and evaporating mini/micro-channel flows [139].

The primary objectives of the present study are to:

(1) Provide a comprehensive survey of previous correlations for condensation heat transfer, dryout incipience quality, and flow boiling heat transfer in both mini/micro-channels and macro-channels.
(2) Review the development of consolidated databases from the world literature for condensing and boiling flows in mini/micro-channels.
(3) Conduct a systematic assessment of previous predictive methods against the consolidated databases.
(4) Discuss the recent development of 'universal' predictive techniques for heat transfer in condensing and boiling flows in mini/micro-channels, which are based on the consolidated databases.

2. Departure from nucleate boiling, dryout, and premature critical heat flux

Before addressing any predictive tools, it is important to point out important limits to flow boiling heat transfer in mini/micro-channels. Critical heat flux (CHF) refers to the heat transfer limit associated an appreciable reduction in the local heat transfer coefficient due to interruption of liquid access to the heated wall. For heat-flux-controlled systems, CHF is associated with a sudden and appreciable rise in wall temperature, with the potential to trigger catastrophic failure of a thermal device. Three different flow boiling CHF mechanisms have been encountered in mini/micro-channel heat sinks: departure from nucleate boiling (DNB), dryout, and premature CHF.

Fig. 4(a) illustrates DNB occurrence in a micro-channel heat sink with D_h = 334.1 μm using HFE-7100 as working fluid [32]. Here, bubbles locally coalesce into a continuous vapor blanket along the heated wall with an abundance of liquid in the core, thus thermally insulating the channel walls from further liquid contact. DNB is more prevalent with high inlet subcoolings, high mass velocities, and small length-to diameter ratios [32].

Dryout is generally associated with saturated inlet conditions or low inlet subcoolings, low mass velocities, and large length-to-diameter ratios. This form of CHF occurs in the annular regime as the liquid film is fully consumed by gradual evaporation, exposing the wall directly to the vapor core. A precursor to this form of CHF is dryout incipience, where local portions of the liquid film begin to dry out. This is shown in Fig. 4(b) for flow boiling of R134a in a heat sink containing rectangular micro-channels [97].

Premature CHF is another important limit for two-phase micro-channel heat sinks, which is associated with significant flow instabilities and oscillations. Fig. 4(c) illustrates premature CHF in the upstream region of a micro-channel heat sink using HFE-7100 as working fluid [32]. Because of low mass velocity and large volume of vapor produced inside the micro-channels, the momentum of incoming liquid in the inlet plenum is momentarily too weak to overcome the pressure drop between the inlet and outlet plenums.

Table 2
Previous annular flow condensation heat transfer correlations and their predictions of 3332 data points of the 4045 consolidated database corresponding to annular condensation in mini/micro-channels ($We^* > 7X_{tt}^{0.2}$) [142].

Author(s)	Equation	Remarks	MAE (%)	θ (%)	ξ (%)
Recommended for macro-channels					
Akers and Rosson [113]	$\frac{h_{tp}D_h}{k_f} = 0.026Pr_f^{1/3}\left\{G\left[(1-x)+x\left(\frac{\rho_f}{\rho_g}\right)^{0.5}\right]\frac{D_h}{\mu_f}\right\}^{0.8}$	D = 19.05 mm R12, propane $Re_g\left(\frac{\mu_g}{\mu_f}\right)\left(\frac{\rho_f}{\rho_g}\right)^{0.5} > 20{,}000,\ Re_f > 5000$	27.3	56.2	93.3
Cavallini and Zecchin [114]	$\frac{h_{tp}D_h}{k_f} = 0.05Re_f^{0.8}Pr_f^{0.33}\left[1+\left(\frac{\rho_f}{\rho_g}\right)^{0.5}\left(\frac{x}{1-x}\right)\right]^{0.8}$	R12, R22, R113 $7000 \leqslant Re_{fo} \leqslant 53{,}000$	56.0	34.9	53.0
Shah [115]	$\frac{h_{tp}D_h}{k_f} = 0.023Re_{fo}^{0.8}Pr_f^{0.4}\left[(1-x)^{0.8}+\frac{3.8x^{0.76}(1-x)^{0.04}}{P_R^{0.38}}\right]$	D = 7–40 mm water, R11, R12, R22, R113, methanol, ethanol, benzene, toluene, trichloroethylene	33.6	64.1	82.8
Haraguchi et al. [116]	$\frac{h_{tp}D_h}{k_f} = 0.0152\left(1+0.6\mathrm{Pr}_f^{0.8}\right)\frac{\phi_g}{X_{tt}}Re_f^{0.77}$ $X_{tt} = \left(\frac{\mu_f}{\mu_g}\right)^{0.1}\left(\frac{1-x}{x}\right)^{0.9}\left(\frac{v_f}{v_g}\right)^{0.5},\ \phi_g = 1+0.5\left[\frac{G}{\sqrt{g\rho_g\left(\rho_f-\rho_g\right)D_h}}\right]^{0.75}X_{tt}^{0.35}$	D = 8.4 mm R22, R123, R134a	94.0	21.0	35.1
Dobson and Chato [117]	$\frac{h_{tp}D_h}{k_f} = 0.023Re_f^{0.8}Pr_f^{0.4}\left(1+\frac{2.22}{X_{tt}^{0.89}}\right)$	D = 3.14–7.04 mm R12, R22, R134a, R32/R125	33.6	56.9	78.3
Moser et al. [118]	$\frac{h_{tp}D_h}{k_f} = \frac{0.0994^{C_1}Re_f^{C_2}Re_{eq}^{1+0.875C_1}\mathrm{Pr}_f^{0.815}}{(1.58\ln Re_{eq}-3.28)\left(2.58\ln Re_{eq}+13.7Pr_f^{2/3}-19.1\right)}$ $C_1 = 0.126Pr_f^{-0.448},$ $C_2 = -0.113Pr_f^{-0.563},\ Re_{eq} = \phi_{fo,Friedel}^{8/7}Re_{fo}$	D = 3.14–20 mm R11, R12, R125, R22, R134a, R410A	27.7	61.8	85.6
Recommended for mini/micro-channels					
Wang et al. [119]	$\frac{h_{tp}D_h}{k_f} = 0.0274Pr_fRe_f^{0.6792}x^{0.2208}\frac{\phi_g}{X_{tt}}$ $\phi_g^2 = 1.376+8X_{tt}^{1.665}$	D_h = 1.46 mm R134a multi-channel	31.5	56.8	82.8
Koyama et al. [120]	$\frac{h_{tp}D_h}{k_f} = 0.0152\left(1+0.6\mathrm{Pr}_f^{0.8}\right)\frac{\phi_g}{X_{tt}}Re_f^{0.77}$ $\phi_g^2 = 1+21[1-\exp(-0.319D_h)]X_{tt}+X_{tt}^2$	D_h = 0.80, 1.11 mm R134a multi-channel	39.0	25.3	74.5
Huang et al. [58]	$\frac{h_{tp}D}{k_f} = 0.0152\left(-0.33+0.83\mathrm{Pr}_f^{0.8}\right)\frac{\phi_g}{X_{tt}}Re_f^{0.77}$ $\phi_g = \phi_{g,Haraguchi}$	D = 1.6, 4.18 mm R410A, R410A/oil	50.5	41.9	63.6
Bohdal et al. [121]	$\frac{h_{tp}D}{k_f} = 25.084Re_f^{0.258}Pr_f^{-0.495}P_R^{-0.288}\left(\frac{x}{1-x}\right)^{0.266}$	D = 0.31–3.30 mm R134a, R404A	70.8	34.3	48.9
Park et al. [60]	$\frac{h_{tp}D}{k_f} = 0.0055Pr_f^{1.37}\frac{\phi_g}{X_{tt}}Re_f^{0.7}$ $\phi_g^2 = 1+13.17\left(\frac{\rho_g}{\rho_f}\right)^{0.17}\left[1-\exp\left(-0.6\sqrt{\frac{g\left(\rho_f-\rho_g\right)D_h^2}{\sigma}}\right)\right]X_{tt}+X_{tt}^2$	D_h = 1.45 mm R134a, R236fa, R1234ze (E) multi-channel	56.3	14.0	24.8

This causes vapor from the micro-channels to flow backwards into the inlet plenum, blocking any incoming liquid from entering the micro-channels, and eventually resulting in dryout and temperature rise in the micro-channels. As discussed in [32], there are two effective means to overcoming premature CHF: increasing mass velocity, to prevent vapor backflow, and increasing inlet subcooling, to reduce bubble growth and coalescence in the inlet plenum.

3. Heat transfer in flow condensation

3.1. Consolidation of world databases for flow condensation in mini/micro-channels

Despite the abundance of correlations to predict two-phase heat transfer in mini/micro-channel flows, most of these correlations have been validated for a relatively small number of working fluids, and narrow ranges of geometrical and flow parameters. To achieve 'universal' correlations that are applicable to the largest number of working fluids and broadest ranges of operating parameters, a series of studies were recently conducted at the Purdue University Boiling and Two-Phase Flow Laboratory (PU-BTPFL). These studies involved systematic consolidation of world databases for mini/micro-channels, and development of universal predictive tools for pressure drop [140,141], heat transfer coefficient [142,143], and dryout incipience quality [144], following closely a methodology that was adopted earlier to predict flow boiling CHF for water flow in tubes [19,145,146].

A total of 4045 data points for flow condensation heat transfer in mini/micro-channels were amassed by the authors of the present study [142] from 28 sources [31,35–61]. Table 1 describes the individual databases comprising the consolidated database, which includes 1964 single-channel data points from 17 sources, and 2081 multi-channel data points from 13 sources. The consolidated database covers a wide range of working fluids, geometrical and flow parameters as presented later.

The condensation data included in Table 1 consist of local or quasi-local heat transfer coefficient data. The data of Wang [40], Baird et al. [42], Matkovic et al. [53], Bortolin [56], Del Col et al. [57], Oh and Son [59], Park et al. [60], and Kim and Mudawar [31] correspond to local heat transfer values. The other condensation data in Table 1 correspond to quasi-local heat transfer

coefficient values, which are averaged over the flow channel length in cases of relatively short lengths or low heat fluxes. Due to small quality decrements, Δx, along the channel, an average of the inlet and outlet qualities is used to determine the quasi-local heat transfer coefficient based on the assumption of linear quality variation along the channel.

3.2. Assessment of previous condensation heat transfer correlations against consolidated database for flow condensation in mini/micro-channels

Table 2 provides a summary of previous condensation heat transfer correlations for annular flow that have been recommended for macro-channels [113–118] and mini/micro-channels [58,60,119–121]. These correlations can be also grouped into the following categories: two-phase multiplier-based correlations [113,115,117], and boundary layer-based correlations [114,116,118,119]. The correlations of Koyama et al. [120], Huang et al. [58], and Park et al. [60] are based on Haraguchi et al.'s formulation. The correlations in Table 2 are intended for uniform circumferential cooling in circular tubes or rectangular channels with four-sided cooling. Following a technique adopted in Refs. [31,93,97], a multiplier is considered to tackle rectangular channels with three-sided wall cooling, such as the data of Derby et al. [61] and Kim and Mudawar [31],

$$h_{tp} = \left(\frac{Nu_3}{Nu_4}\right) h_{tp,cir}, \tag{1}$$

where $h_{tp,cir}$ is the local heat transfer coefficient based on uniform circumferential cooling obtained from Table 2, and Nu_3 and Nu_4 are Nusselt numbers for thermally developed laminar flow with three-sided and four-sided heat transfer [147], respectively,

$$Nu_3 = 8.235(1 - 1.833\ \beta + 3.767\beta^2 - 5.814\beta^3 + 5.361\beta^4 - 2.0\beta^5) \tag{2a}$$

and

$$Nu_4 = 8.235(1 - 2.042\beta + 3.085\beta^2 - 2.477\beta^3 + 1.058\beta^4 - 0.186\beta^5). \tag{2b}$$

Table 2 shows predictions of previous correlations of mini/micro-channel annular flow data corresponding to 3332 data points of the 4045 consolidated database, where the annular data are identified using a flow regime map by the present authors [31]. As shown in [31,139], flow regime transition between annular and intermittent condensing, adiabatic, and boiling mini/micro-channel flows is predicted well by the boundary of $We^* = 7X_{tt}^{0.2}$, where the modified Weber number is defined by Soliman [148] as

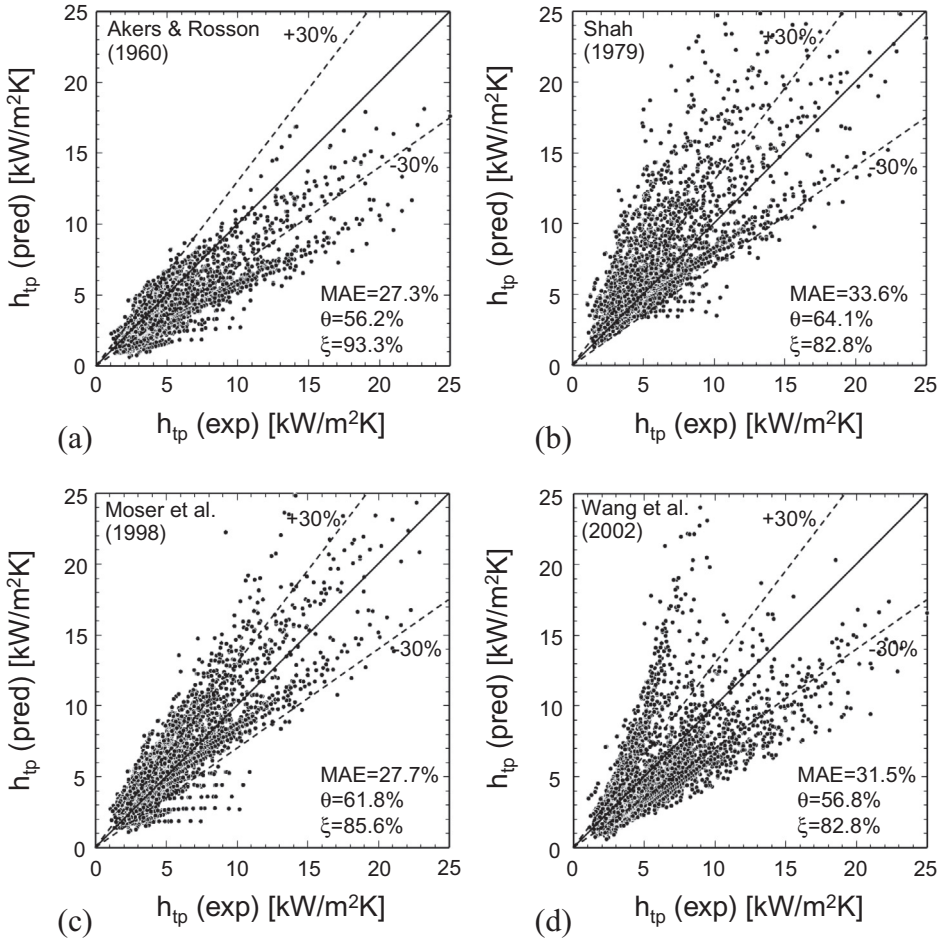

Fig. 5. Comparison of 3332 data points of the 4045 point consolidated database corresponding to annular condensation in mini/micro-channels ($We^* > 7X_{tt}^{0.2}$) with predictions of annular flow condensation correlations: (a) Akers and Rosson [113], (b) Shah [115], (c) Moser et al. [118], and (d) Wang et al. [119] (adapted from [142]).

Table 3
Universal condensation heat transfer correlation for mini/micro-channels in both single and multi-channel configurations [142]. The pressure drop predictions are based on Ref. [140].

$h_{tp} = \left(\frac{Nu_3}{Nu_4}\right) h_{tp,cir}$

for annular flow where $We^* > 7X_{tt}^{0.2}$:

$\frac{h_{tp,cir} D_h}{k_f} = 0.048\,\mathrm{Re}_f^{0.69}\,\mathrm{Pr}_f^{0.34}\,\frac{\phi_g}{X_{tt}}$

for slug and bubbly flows where $We^* < 7X_{tt}^{0.2}$:

$\frac{h_{tp,cir} D_h}{k_f} = \left[\left(0.048 Re_f^{0.69} Pr_f^{0.34} \frac{\phi_g}{X_{tt}}\right)^2 + \left(3.2\times10^{-7} Re_f^{-0.38} Su_{go}^{1.39}\right)^2\right]^{0.5}$

where h_{tp} is local heat transfer coefficient for rectangular channels with three-sided cooling, and $h_{tp,cir}$ is local heat transfer coefficient for uniform circumferential cooling in circular tubes or rectangular channels with four-sided cooling

where $X_{tt} = \left(\frac{\mu_f}{\mu_g}\right)^{0.1}\left(\frac{1-x}{x}\right)^{0.9}\left(\frac{\rho_g}{\rho_f}\right)^{0.5}$

$\phi_g^2 = 1 + CX + X^2,\ X^2 = \frac{(dp/dz)_f}{(dp/dz)_g}$

$-\left(\frac{dp}{dz}\right)_f = \frac{2f_f v_f G^2 (1-x)^2}{D_h},\ -\left(\frac{dp}{dz}\right)_g = \frac{2f_g v_g G^2 x^2}{D_h}$

$f_k = 16Re_k^{-1}$ for $Re_k < 2000$

$f_k = 0.079Re_k^{-0.25}$ for $2000 \leqslant Re_k < 20{,}000$

$f_k = 0.046Re_k^{-0.2}$ for $Re_k \geqslant 20{,}000$

for laminar flow in rectangular channel ($\beta < 1$),

$f_k Re_k = 24\left(1 - 1.3553\beta + 1.9467\beta^2 - 1.7012\beta^3 + 0.9564\beta^4 - 0.2537\beta^5\right)$

where subscript k denotes f or g for liquid and vapor phases, respectively

$Re_f = \frac{G(1-x)D_h}{\mu_f},\ Re_g = \frac{GxD_h}{\mu_g},\ Re_{fo} = \frac{GD_h}{\mu_f},\ Su_{go} = \frac{\rho_g \sigma D_h}{\mu_g^2}$

	C
$Re_f \geqslant 2000$, $Re_g \geqslant 2000$ (tt)	$0.39Re_{fo}^{0.03} Su_{go}^{0.10}\left(\frac{\rho_f}{\rho_g}\right)^{0.35}$
$Re_f \geqslant 2000$, $Re_g < 2000$ (tv)	$8.7\times10^{-4} Re_{fo}^{0.17} Su_{go}^{0.50}\left(\frac{\rho_f}{\rho_g}\right)^{0.14}$
$Re_f < 2000$, $Re_g \geqslant 2000$ (vt)	$0.0015 Re_{fo}^{0.59} Su_{go}^{0.19}\left(\frac{\rho_f}{\rho_g}\right)^{0.36}$
$Re_f < 2000$, $Re_g < 2000$ (vv)	$3.5\times10^{-5} Re_{fo}^{0.44} Su_{go}^{0.50}\left(\frac{\rho_f}{\rho_g}\right)^{0.48}$

Correlation based on consolidated database of 4045 condensation heat transfer data points from 28 sources with the following application range:
- working fluid: R12, R123, R1234yf, R1234ze (E), R134a, R22, R236fa, R245fa, R32, R404A, R410A, R600a, FC72, methane, and CO_2
- hydraulic diameter: $0.424 < D_h < 6.22$ mm
- mass velocity: $53 < G < 1403$ kg/m^2 s
- liquid-only Reynolds number: $276 < Re_{fo} = G\,D_h/\mu_f < 89{,}798$
- superficial liquid Reynolds number: $0 < Re_f = G(1-x)D_h/\mu_f < 79{,}202$
- superficial vapor Reynolds number: $0 < Re_g = G\,x\,D_h/\mu_g < 247{,}740$
- flow quality: $0 < x < 1$
- reduced pressure: $0.04 < P_R < 0.91$.

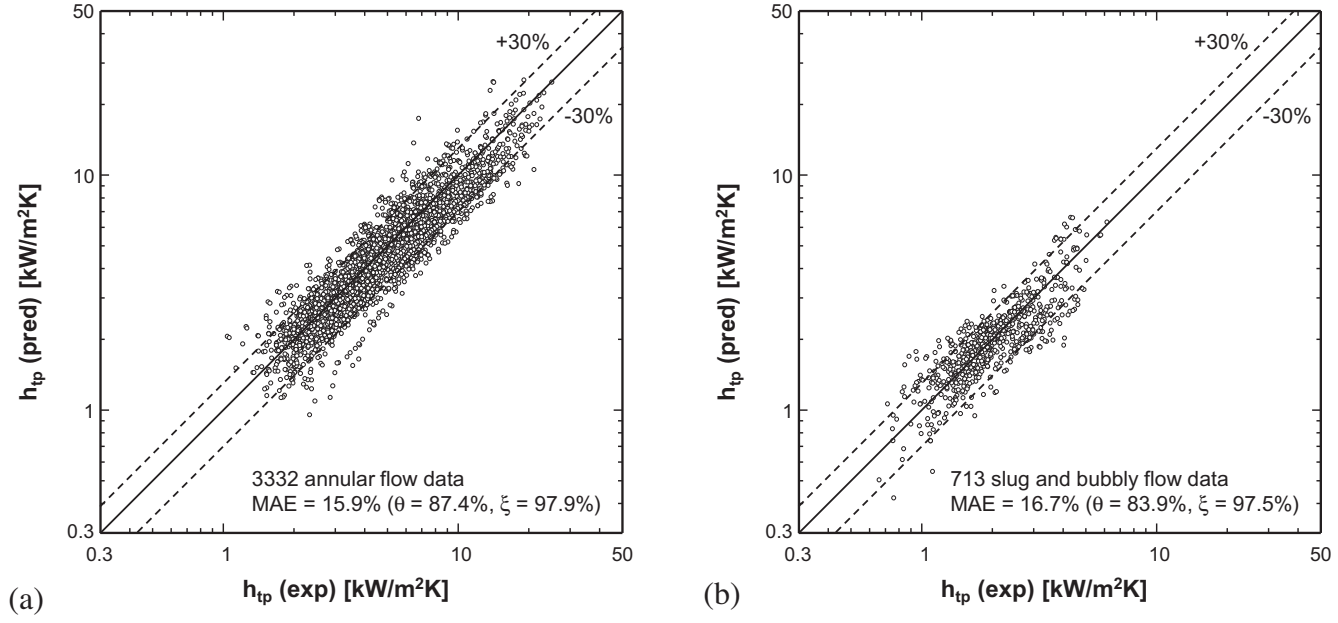

Fig. 6. Comparison of predictions of universal condensation heat transfer correlations with two subsets of the 4045 point consolidated database corresponding to: (a) annular flow data and (b) slug and bubbly flow data (adapted from [142]).

$$We^* = 2.45\frac{Re_g^{0.64}}{Su_{go}^{0.3}\left(1+1.09X_{tt}^{0.039}\right)^{0.4}} \quad \text{for } Re_f \leqslant 1250 \tag{3a}$$

and

$$We^* = 0.85\frac{Re_g^{0.79}X_{tt}^{0.157}}{Su_{go}^{0.3}\left(1+1.09X_{tt}^{0.039}\right)^{0.4}}\left[\left(\frac{\mu_g}{\mu_f}\right)^2\left(\frac{v_g}{v_f}\right)\right]^{0.084} \quad \text{for } Re_f > 1250. \tag{3b}$$

Thermophysical properties for different fluids are evaluated using NIST's REFPROP 8.0 software [149], excepting those for FC-72, which are obtained from 3 M Company. Three different parameters are used to assess the accuracy of individual models or correlations. θ and ξ are defined as the percentages of data points predicted within ±30% and ±50%, respectively, and MAE the mean absolute error, which is determined according to

$$MAE = \frac{1}{N}\sum\frac{|h_{tp,pred} - h_{tp,exp}|}{h_{tp,exp}} \times 100\%. \tag{4}$$

Overall, relatively good predictions are achieved using the correlations of Akers and Rosson [113] and Moser et al. [118], evidenced by MAE values of 27.3% and 27.7%, respectively.

Fig. 5(a)–(d) compare the 3332 experimental mini/micro-channel annular flow condensation data points with predictions of select correlations that have shown relatively superior predictive capability. The correlations of Akers and Rosson [113] and Wang et al. [119] generally underpredict a large fraction of the database, with some scatter by Wang et al. The correlations of Shah [115] and Moser et al. [118] overpredict most of the database, especially for high pressures.

Table 4
Comparison of individual mini/micro-channel condensation heat transfer databases with predictions of universal correlation for mini/micro-channels and select previous correlations [142].

Author(s)	Fluid(s)	Mean absolute error (%)								
		Annular flow data[a]						Slug and bubbly flow data		
		Data points	Akers and Rosson [113]	Shah [115]	Moser et al. [118]	Wang et al. [119]	Universal correlation Eq. (8)	Data points	Shah [122]	Universal correlation Eq. (9)
Dobson et al. [35]	R134a, R12	73	28.7	8.2	17.6	29.8	13.3	3	19.2	2.9
Dobson et al. [36]	R22	29	36.8	9.4	17.1	44.0	20.8	3	13.9	8.7
Dobson et al. [37]	R134a, R22	150	40.4	12.5	12.8	44.3	27.3	15	15.3	16.2
Hirofumi and Webb [38]	R134a	61	12.9	41.0	39.1	12.3	14.6	1	29.9	5.1
Zhang [39]	R134a, R22, R404A	79	31.0	11.4	10.5	33.0	21.3	1	3.8	1.8
Wang [40]	R134a	524	13.4	29.4	30.0	9.4	7.4	224	42.0	12.7
Yan and Lin [41]	R134a	60	40.3	10.6	12.1	21.0	11.3	18	18.5	13.9
Baird et al. [42]	R123	140	24.3	16.7	24.1	47.8	30.0	3	7.1	7.4
Kim et al. [43]	R410A, R22	19	13.1	28.7	28.5	16.8	8.9	–	–	–
Jang and Hrnjak [44]	CO_2	78	16.1	22.9	32.9	32.1	10.8	7	7.7	13.0
Cavallini et al. [45]	R410A, R134a	56	30.3	14.9	12.7	33.4	19.1	3	7.0	13.6
Mitra [46]	R410A	144	24.1	101.4	56.2	34.6	12.0	–	–	–
Shin and Kim [47]	R134a	160	37.5	14.2	19.6	20.6	17.7	77	31.4	26.0
Andresen [48]	R410A	312	23.8	108.8	55.2	47.9	16.0	3	69.1	68.1
Bandhauer et al. [49]	R134a	116	25.9	13.0	15.1	15.1	10.0	12	30.6	15.6
Agra and Teke [50]	R600a	50	46.6	48.0	16.6	17.5	13.3	–	–	–
Kim et al. [51]	CO_2	42	15.8	27.6	39.1	25.9	15.6	6	31.2	12.6
Marak [52]	methane	124	14.9	37.5	24.2	32.0	12.4	5	25.3	8.3
Matkovic et al. [53]	R134a, R32	131	32.7	14.4	14.0	34.5	15.6	30	26.6	11.4
Park and Hrnjak [54]	CO_2	78	13.1	33.5	43.5	13.9	26.7	35	39.1	20.9
Agarwal et al. [55]	R134a	38	23.9	22.2	25.2	13.5	13.5	5	51.6	24.4
Bortolin [56]	R245fa, R134a	241	43.1	17.7	13.6	30.0	22.4	68	20.9	17.7
Del Col et al. [57]	R1234yf	56	27.5	6.1	8.6	16.3	9.1	10	12.8	10.0
Huang et al. [58]	R410A	35	37.7	14.5	15.7	48.0	31.6	–	–	–
Oh and Son [59]	R22, R134a, R410A	108	31.4	23.6	24.1	33.6	25.1	–	–	–
Park et al. [60]	R134a, R236fa, R1234ze	117	20.0	38.6	30.8	18.4	19.1	87	21.3	15.0
Derby et al. [61]	R134a	72	24.2	22.5	28.0	10.1	12.9	68	30.8	22.1
Kim and Mudawar [31]	FC-72	239	44.7	18.4	30.4	86.6	11.8	29	19.4	19.6
Total		3332	27.3	33.6	27.7	31.5	15.9	713	30.8	16.7

[a] Annular flow data (smooth-annular, wavy-annular and transition to slug) corresponding to $We^* > 7X_{tt}^{0.2}$.

3.3. Universal predictive method based on consolidated database for flow condensation in mini/micro-channels

For shear-dominated annular condensing flow, the local condensation heat transfer coefficient of the liquid film can be obtained from the following relation [31],

$$h_{ann} = \frac{q''_H}{T_{sat} - T_w} = \frac{\rho_f c_{p,f} u^*}{T_\delta^+}, \tag{5}$$

where the friction velocity and dimensionless boundary layer temperature are defined, respectively, as

$$u^* = \sqrt{\tau_w / \rho_f} \tag{6}$$

and

$$T_\delta^+ = \int_0^{\delta^+} \frac{q''}{q''_H} \left(\frac{1}{Pr_f} + \frac{1}{Pr_T} \frac{\varepsilon_m}{\nu_f} \right)^{-1} dy^+. \tag{7}$$

Using Lockhart and Martinelli's [150] two-phase multiplier, and the functional forms of $T_\delta^+ = f(Re_f, Pr_f)$ proposed by Dobson and Chato [117] and Traviss et al. [151], yields the following universal correlation for local heat transfer coefficient for annular condensing flow [12],

$$\frac{h_{ann} D_h}{k_f} = 0.048 Re_f^{0.69} Pr_f^{0.34} \frac{\phi_g}{X_{tt}}, \tag{8}$$

where the coefficient and two exponents are obtained by fitting 3332 data points of the consolidated 4045 point mini/micro-channel condensation database corresponding to $We^* > 7X_{tt}^{0.2}$. The universal two-phase frictional pressure gradient correlation for adiabatic and condensing mini/micro-channel flows proposed by Kim and Mudawar [140] is used to determine ϕ_g and the constant C in the Lockhart–Martinelli parameter as shown in Table 3. Fig. 6(a) shows the universal local heat transfer coefficient correlation for annular condensing flows predicts the 3332 annular data points with a MAE of 15.9%,

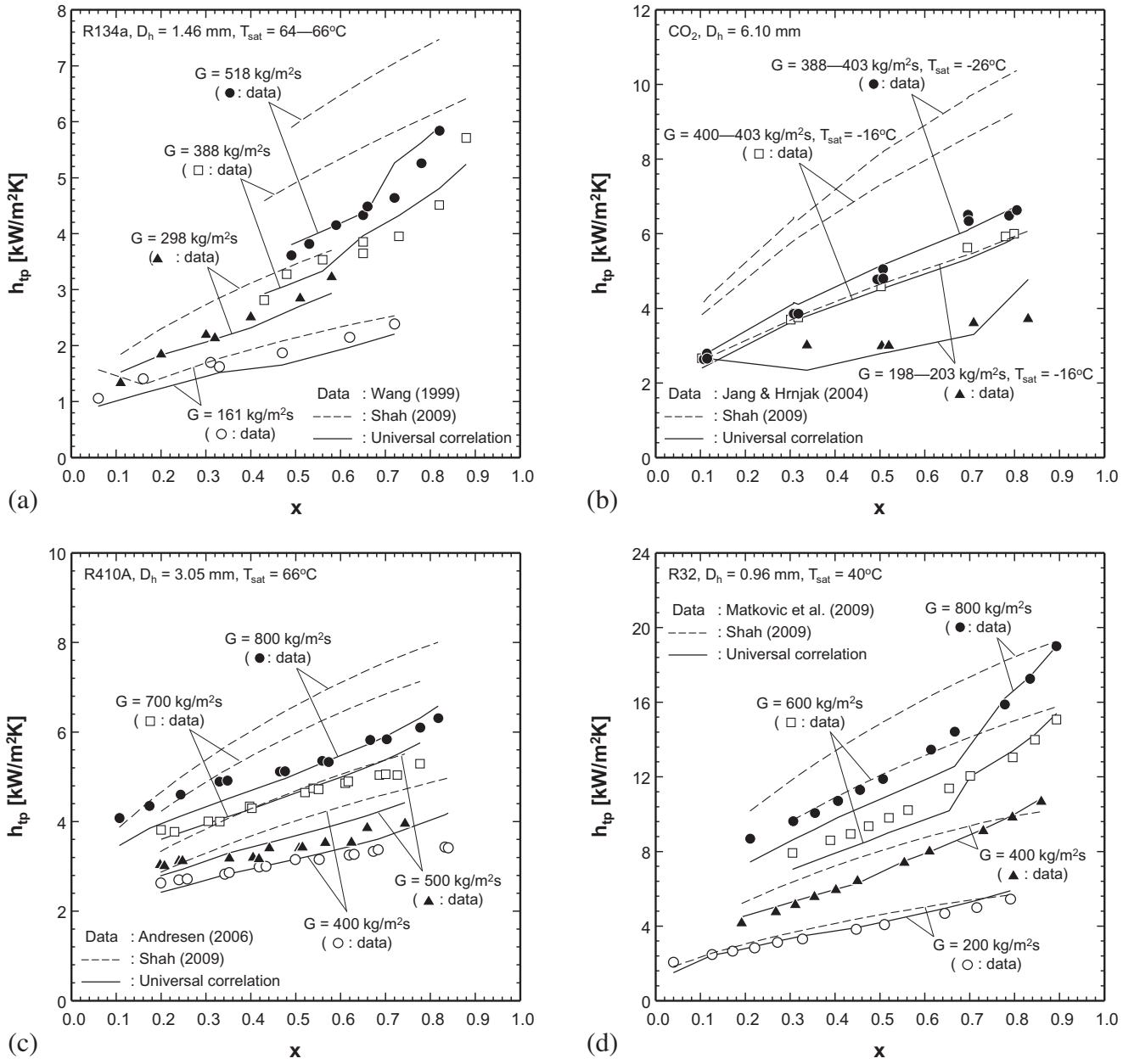

Fig. 7. Comparison of predictions of universal condensation heat transfer correlations and Shah's correlation [122] with experimental data for condensing mini/micro-channel flow by (a) Wang [40], (b) Jang and Hrnjak [44], (c) Andresen [48], and (d) Matkovic et al. [53].

Table 5
Consolidated database for saturated boiling mini/micro-channel flows used to develop universal dryout incipience quality correlation [144].

Author(s)	Channel geometry[a]	Channel material	D_h [mm]	Relative roughness, e/D_h	Fluid(s)	G (kg/m^2 s)	Data points	Remarks[b]
Becker [62]	C, single, VU	–	2.4, 3.0	–	Water	365–2725	82	x_{crit} identified by fast increase of T_w
Lezziet al. [63]	C, single, H	Stainless steel	1.0	Smooth	Water	776–2738	68	x_{crit} identified by fast increase of T_w of 5 °C
Baek and Chang [64]	C, single, VU	Stainless steel	6.0	–	Water	29–277	232	x_{crit} identified by fast increase of T_w when T_w > 250 °C
Roach et al. [65]	C, single, H	Copper	1.168, 1.448	0.0017, 0.0014	Water	256–1037	42	x_{crit} identified by fast increase of T_w when T_w > 250 °C
Kim et al. [66]	C, single, VU	Inconel-625	6.0	–	Water	99–277	210	x_{crit} identified by fast increase of T_w with T_w increase rate of 50 °C/s
Yang and Fujita [67]	R, single, H	Copper bottom, Pyrex cover	0.976	–	R113	100, 200	3	x^*_{di} identified by falling off of h_{tp}
Yu et al. [68]	C, single, H	Stainless steel	2.98	–	Water	50–151	30	x_{crit} identified by fast increase of T_w
Saitoh et al. [69]	C, single, H	Stainless steel	0.51, 1.12, 3.1	Smooth	R134a	150–300	41	x^*_{di} identified by falling off of h_{tp}
Yun et al. [70]	R, multi, H	Stainless steel	1.14	–	CO_2	300, 400	2	x^*_{di} identified by falling off of h_{tp}
Hihara and Dang [71]	C, single, H	Stainless steel	1.0, 2.0, 4.0, 6.0	Smooth	CO_2	360–1440	16	x_{di} identified by falling off of h_{tp}
Greco [72]	C, single, H	Stainless steel	6.0	Smooth	R134a, R22, R407C, R410A	199–1079	7	x^*_{di} identified by falling off of h_{tp}
Shiferaw [73]	C, single, VU	Stainless steel	1.1, 2.88, 4.26	0.0012, 0.0005, 0.0004	R134a	200–400	13	x^*_{di} identified by falling off of h_{tp}
Ohta et al. [74]	C, single, H	Stainless steel	0.51	–	FC72	107, 215	2	x^*_{di} identified by falling off of h_{tp}
Wang et al. [75]	C, single, H	Stainless steel	1.3	–	R134a	321–676	9	x^*_{di} identified by falling off of h_{tp}
Martín-Callizo [76]	C, single, VU	Stainless steel	0.64	0.0012	R134a, R22, R245fa	185–541	42	x_{di} identified by change of slope in boiling curve, and wall temperature fluctuation from $T_{w,std}$
Ali and Palm [77]	C, single, VU	Stainless steel	1.22, 1.70	0.0021, 0.0001	R134a	50–600	23	x_{di} identified by change of slope in boiling curve, and wall temperature fluctuation from $T_{w,std}$
Ducoulombier et al. [78]	C, single, H	Stainless steel	0.529	0.0015–0.0030	CO_2	200–1410	48	x_{di} identified by falling off of h_{tp}
Oh and Son [79]	C, single, H	Copper	1.77, 3.36, 5.35	Smooth	R134a, R22	200–400	6	x^*_{di} identified by falling off of h_{tp}
Oh and Son [80]	C, single, H	Stainless steel	4.57	Smooth	CO_2	600–900	8	x^*_{di} identified by falling off of h_{tp}
Oh et al. [81]	C, single, H	Stainless steel	1.5, 3.0	Smooth	R22, R410A, R290	100–500	9	x^*_{di} identified by falling off of h_{tp}
Wu et al. [82]	C, single, H	Stainless steel	1.42	–	CO_2	300–600	18	x^*_{di} identified by falling off of h_{tp}
Del Col and Bortolin [83]	C, single, H	Copper	0.96	0.0014	R134a, R245fa, R32	101–902	43	x_{di} identified by wall temperature fluctuation from $T_{w,std}$
Karayiannis et al. [84]	C, single, VU	Stainless steel	1.1	0.0012	R134a	300	3	x_{di} identified by falling off of h_{tp}
Li et al. [85]	C, single, H	Stainless steel	2.0	Smooth	R1234yf, R32	100–400	8	x^*_{di} identified by falling off of h_{tp}
Mastrullo et al. [86]	C, single, H	Stainless steel	6.0	$\leqslant$ 0.00007	CO_2, R410A	150–501	28	x_{di} identified by falling off of h_{tp}
Tibiriçá et al. [87]	C, single, H	Stainless steel	1.0	0.0006	R1234ze	300–600	4	x^*_{di} identified by falling off of h_{tp}
Total							997	

[a] C: circular, R: rectangular, H: horizontal, VU: vertical upflow.
[b] x_{crit}: critical quality data reported by original authors, x_{di}: dryout incipience quality data reported by original authors, x^*_{di}: dryout incipience quality data identified by present authors by falling off in measured two-phase heat transfer coefficient attributed by original authors to dryout incipience.

with 87.4% and 97.9% of the data falling within ±30% and ±50% error bands, respectively.

For slug and bubbly flows, a superposition of the Churchill and Usagi [152] type of the universal annular flow heat transfer correlation, Eq. (8), and a dimensionless function of the superficial liquid Reynolds number, Re_f, and vapor-only Suratman number, Su_{go}, are used. Based on 713 slug and bubbly flow data points of the 4045 data points of the consolidated database corresponding to $We^* < 7\text{-}X_{tt}^{0.2}$, the following universal condensation heat transfer correlation for the slug and bubbly flow regimes [142] is derived by regression analysis,

$$\frac{h_{non-ann}D_h}{k_f} = \left[\left(\frac{h_{ann}D_h}{k_f}\right)^2 + \left(3.2\times10^{-7}Re_f^{-0.38}Su_{go}^{1.39}\right)^2\right]^{0.5}. \quad (9)$$

Fig. 6(b) shows the universal local heat transfer coefficient correlation for slug and bubbly flows predicts the 713 slug and bubbly flow data with a MAE of 16.7%, with 83.9% and 97.5% of the data falling within ±30% and ±50% error bands, respectively.

To further examine the predictive accuracy of the universal correlation, individual mini/micro-channel databases from 28 sources are compared in Table 4 with predictions of the universal correlation as well as select previous correlations. For the annular flow

Table 6
Previous correlations for dryout incipience quality, and their predictions of entire 997-point consolidated database for mini/micro-channel flows [144].

Author(s)	Equation	Remarks	MAE[a] (%)	θ (%)	ξ (%)
Sun [123]	$x_{crit} = 10.795(q''_H/1000)^{-0.125}G^{-0.333}(1000D_h)^{-0.07}\exp\left(0.01715\times10^{-5}p\right)$ for $4.9 \leqslant p \leqslant 29.4$ bar, $x_{crit} = 19.398(q''_H/1000)^{-0.125}G^{-0.333}(1000D_h)^{-0.07}\exp\left(-0.00255\times10^{-5}p\right)$ for $29.4 \leqslant p \leqslant 98$ bar, $x_{crit} = 32.302(q''_H/1000)^{-0.125}G^{-0.333}(1000D_h)^{-0.07}\exp\left(-0.00795\times10^{-5}p\right)$ for $98 \leqslant p \leqslant 196$ bar, $Fr^* = \frac{x_{crit}G}{\sqrt{\rho_g(\rho_f-\rho_g)g\cos\theta D_h}}$, $\theta = 0$ for horizontal flow, $x_{di} = x_{crit} - \frac{8}{(2+Fr^*)^2}$, q''_H in (W/m^2), G in (kg/m^2 s), D_h in (m), p in (Pa)	D = 4.572 mm, CO_2	45.0	56.9	70.6
Yoon et al. [124]	$x_{di} = 0.0012Re_{fo}^{2.79}(1000Bo)^{0.06}Bd^{-4.76}$, $Re_{fo} = \frac{GD_h}{\mu_f}$, $Bo = \frac{q''_H}{Gh_{fg}}$, $Bd = \frac{g(\rho_f-\rho_g)D_h^2}{\sigma}$	D = 7.53 mm, CO_2	–	0.7	1.0
Wojtan et al. [125]	$x_{di} = 0.58\exp\left[0.52 - 0.235We_g^{0.17}Fr_{g,Mori}^{0.37}\left(\frac{\rho_g}{\rho_f}\right)^{0.25}\left(\frac{q''_H}{q''_{crit}}\right)^{0.70}\right]$, $We_g = \frac{G^2D_{eq}}{\rho_g\sigma}$, $Fr_{g,Mori} = \frac{G^2}{\rho_g(\rho_f-\rho_g)gD_{eq}}$, $D_{eq} = \sqrt{\frac{4A}{\pi}}$, $q''_{crit} = 0.131\rho_g^{0.5}h_{fg}\left[g\sigma(\rho_f-\rho_g)\right]^{0.25}$	D = 8.00, 13.84 mm, R22, R410A	41.8	46.3	66.4
Cheng et al. [126]	$x_{di} = 0.58\exp\left[0.52 - 0.67We_g^{0.17}Fr_{g,Mori}^{0.348}\left(\frac{\rho_g}{\rho_f}\right)^{0.25}\left(\frac{q''_H}{q''_{crit}}\right)^{0.70}\right]$	D_h = 0.8–10.06 mm, CO_2	64.4	20.0	33.2
Del Col et al. [127]	$x_{di} = 0.4695\left(\frac{4q''_H RLL}{GD_h h_{fg}}\right)^{1.472}\left(\frac{G^2D_h}{\rho_f\sigma}\right)^{0.3024}\left(\frac{D_h}{0.001}\right)^{0.1836}(1-P_R)^{1.239}$, $RLL = \left[0.437\left(\frac{\rho_g}{\rho_f}\right)^{0.073}\left(\frac{\rho_f\sigma}{G^2}\right)^{0.24}D_h^{0.72}\left(\frac{Gh_{fg}}{q''_H}\right)\right]^{1/0.96}$, D_h in (m)	Mini-channels, refrigerants, CO_2	27.0	64.3	91.7
Cheng et al. [128]	$x_{di} = 0.58\exp\left[0.52 - 0.236We_g^{0.17}Fr_{g,Mori}^{0.17}\left(\frac{\rho_g}{\rho_f}\right)^{0.25}\left(\frac{q''_H}{q''_{crit}}\right)^{0.27}\right]$	D_h = 0.6–10.06 mm, CO_2	24.2	74.2	82.4
Jeong and Park [129]	$x_{di} = 6.2Re_{fo}^{-0.5}Bo^{-0.2}Bd^{-0.45}$	D = 0.80, 0.81 mm, CO_2	73.6	10.4	19.8
Ducoulombier et al. [78]	$x_{di} = 1 - 338Bo^{0.703}P_R^{1.43}$	D = 0.529 mm, CO_2	31.7	55.9	81.6
Mastrullo et al. [86]	$x_{di} = 1 - 20.82q''^{0.273}_H G^{1.231}D_h^{0.252}\frac{\mu_f}{h_{fg}^{0.273}(\rho_f\sigma)^{1.252}}P_R^{-0.721}$, q''_H in (W/m^2), G in (kg/m^2 s), D_h in (m)	D = 6.00 mm, R410A, CO_2	24.1	73.3	89.7

[a] Dash indicates mean absolute error $\gg$ 100%.

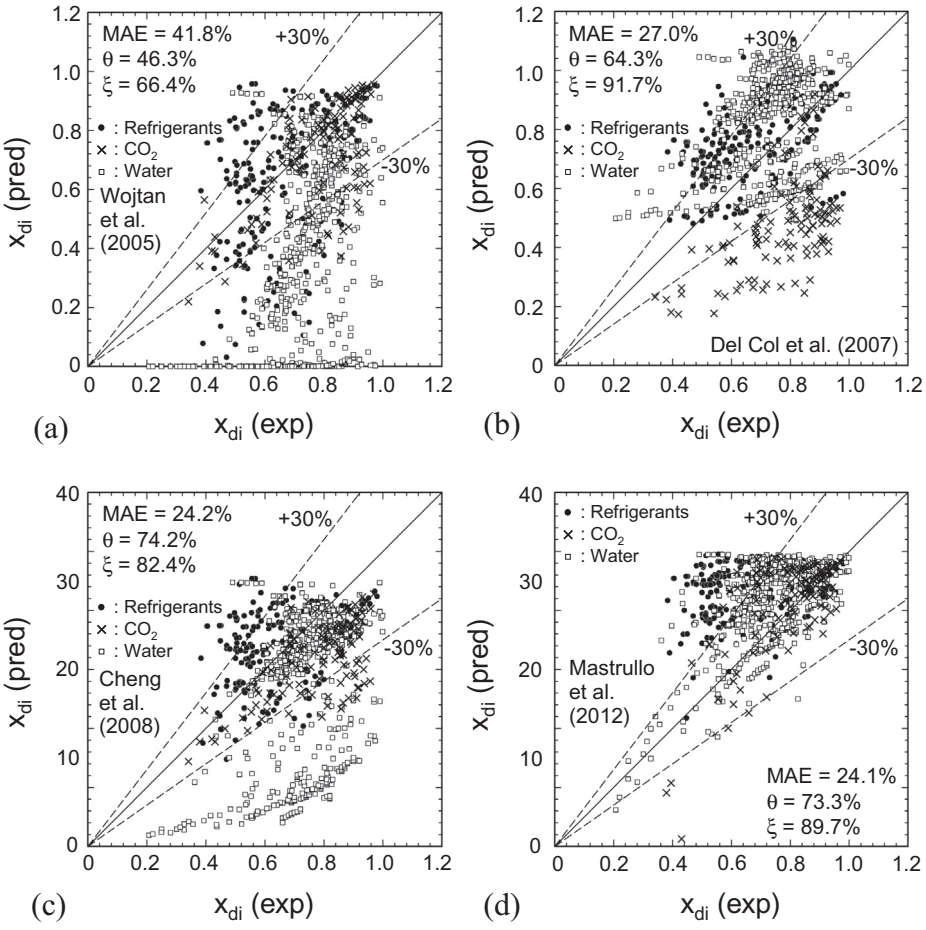

Fig. 8. Comparison of 997 point consolidated database for dryout incipience with predictions of correlations of (a) Wojtan et al. [125], (b) Del Col et al. [127], (c) Cheng et al. [128], and (d) Mastrullo et al. [86] (adapted from [144]).

Table 7
Universal dryout incipience quality correlation for saturated boiling mini/micro-channel flows [144].

$$x_{di} = 1.4We_{fo}^{0.03}P_R^{0.08} - 15.0\left(Bo\frac{P_H}{P_F}\right)^{0.15}Ca^{0.35}\left(\frac{\rho_g}{\rho_f}\right)^{0.06}$$

where $We_{fo} = \frac{G^2 D_h}{\rho_f \sigma}$, $P_R = \frac{p}{p_{crit}}$, $Bo = \frac{q''_H}{Gh_{fg}}$, $Ca = \frac{\mu_f G}{\rho_f \sigma} = \frac{We_{fo}}{Re_{fo}}$,

q''_H: effective heat flux averaged over heated perimeter of channel,
P_H: heated perimeter of channel, P_F: wetted perimeter of channel
Correlation based on consolidated database of 997 dryout data points from 26 sources with the following application range:

- Working fluid: FC72, R113, R1234yf, R1234ze, R134a, R22, R245fa, R290, R32, R407C, R410A, CO_2, and water
- Hydraulic diameter: $0.51 < D_h < 6.0$ mm
- Mass velocity: $29 < G < 2303$ kg/m^{2}s
- Liquid-only Reynolds number: $125 < Re_{fo} = G\,D_h/\mu_f < 53{,}770$
- Boiling number: $0.31 \times 10^{-4} < Bo = q''_H/Gh_{fg} < 44.3 \times 10^{-4}$
- Reduced pressure: $0.005 < P_R < 0.78$

data, the universal annular flow correlation, Eq. (8), provides excellent predictive capability against all individual databases, with 11 databases predicted more accurately than by any of the select previous correlations, and the best overall MAE of 15.9%. For the slug and bubbly flow data, the individual databases are compared with predictions of the universal correlation for slug and bubbly flow, Eq. (9), and Shah's [122] generalized correlation, which is an improved version of his original annular flow correlation [115]. With a MAE of 16.7%, the universal correlation provides excellent predictions for all individual databases excluding the three data points of Andresen [48], which exhibit strong departure from the majority of comparable data.

Predictions of the universal correlation and Shah's [122] recent correlation are compared in Fig. 7(a)–(d) with representative mini/micro-channel experimental data [40,44,48,53]. The Shah correlation overpredicts most of the experimental data. In contrast, the universal correlation accurately captures experimental data in both magnitude and trend; h_{tp} increases with increasing flow quality and mass velocity, and decreases with increasing saturation temperature.

4. Dryout incipience quality in flow boiling

4.1. Consolidation of world databases for dryout incipience quality in mini/micro-channels

In their study of dryout incipience [144], the authors of the present study amassed a total of 997 mini/micro-channel data points for dryout incipience quality, x_{di}, and critical quality, x_{crit}, at which CHF occurs from 26 sources [62–87]. Table 5 describes the individual databases comprising the consolidated database, which include 664 critical quality data points for water from 6 sources, and 333 dryout incipience quality data points for other fluids from 20 sources. The consolidated database covers a wide range of working fluids, geometrical and flow parameters as presented later.

The 664 water data of Becker [62], Lezzi et al. [63], Baek and Chang [64], Roach et al. [65], Kim et al. [66], and Yu et al. [68] correspond to the critical quality at which CHF occurs. Notice that different criteria are adopted by individual authors to determine CHF. The CHF criterion of Lezzi et al. is more closely related to dryout incipience because the critical quality is identified by a 5 °C increase in average wall temperature following a small heat flux increment and long waiting period. In contrast, the CHF criterion of Baek and Chang is indicative of dryout completion, or true CHF, because the critical quality is identified when the wall temperature exceeds a fairly high limit of 250°C. As discussed by the present authors [144], the dryout incipience and dryout completion conditions are quite close for water, which is why the critical quality data for water in Table 5 are used to represent data for dryout incipience quality in the development of the universal correlation for dryout incipience quality.

The 333 dryout incipience quality data for fluids other than water consist of 203 dryout incipience quality data points as reported by the original authors, and 130 dryout incipience quality data points identified by the falling off in measured two-phase heat transfer coefficient attributed by the original authors to dryout incipience.

4.2. Assessment of previous correlations against the consolidated database for dryout incipience quality in mini/micro-channels

Table 6 provides a summary of previous correlations for dryout incipience quality, x_{di}, [78,86,123–129] and their predictions of the entire 997-point consolidated database for mini/micro-channel flows, where the mean absolute error is calculated from Eq. (4) by replacing h_{tp} with x_{di}. Notice that the correlations of Cheng et al. [126,128], Del Col et al. [127], Jeong and Park [129], and Ducoulombier et al. [78] are intended specifically for mini/micro-channel flows. The correlations of Wojtan et al. [125] and Cheng et al. [126,128] are based on a functional formulation by Mori et al. [153], and the correlation of Jeong and Park on a functional formulation by Yoon et al. [124]. Overall, relatively good predictions are achieved with the correlations of Cheng et al. [128] and Mastrullo et al. [86], with MAE values of 24.2% and 24.1%, respectively.

Fig. 8(a)–(d) compare the entire 997-point mini/micro-channel consolidated database with predictions of select previous correlations for dryout incipience quality, x_{di}, that have shown relatively superior predictive capability, by segregating data into three fluid subsets of refrigerants, CO_2, and water. A large fraction of the water

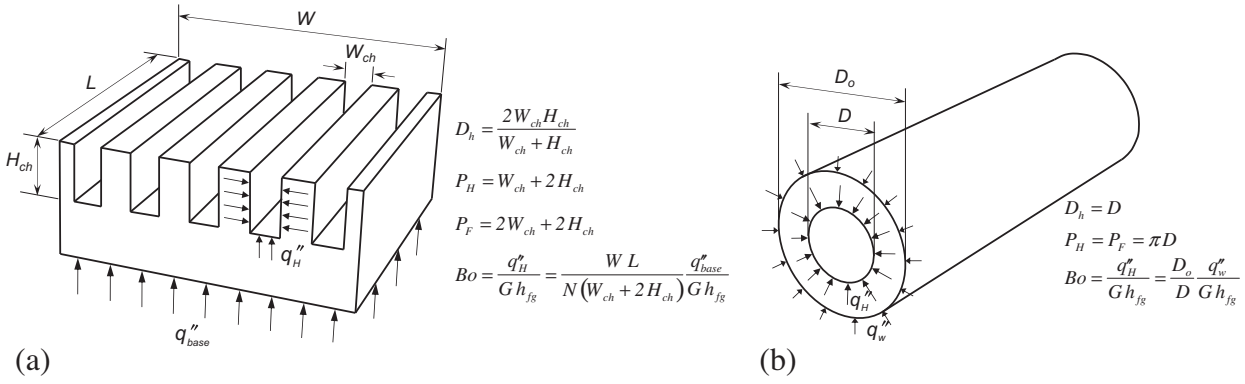

Fig. 9. (a) Rectangular multi-channel heat sink with three-sided wall heating, and (b) circular single channel with uniform circumferential wall heating.

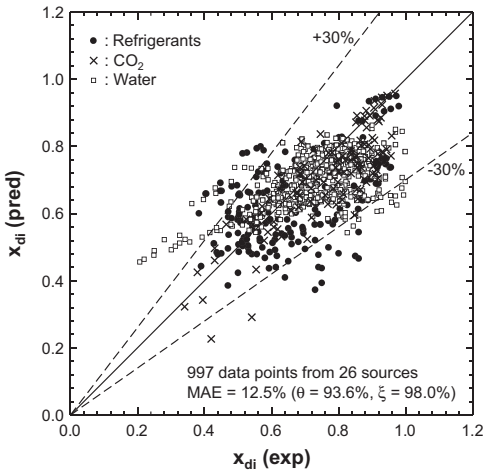

Fig. 10. Comparison of predictions of universal dryout incipience quality correlation with consolidated 997 point database for mini/microchannels (adapted from [144]).

data are highly underpredicted by the correlations of Wojtan et al. [125] and Cheng et al. [128]. Most of the CO_2 data are significantly underpredicted by the correlation of Del Col et al. [127]. The correlation of Mastrullo et al. [86] provides better MAE than all other eight correlations, although it overpredicts a large fraction of the refrigerants and water data.

4.3. Universal predictive method based on consolidated database for dryout incipience quality in mini/micro-channels

A universal correlation for dryout incipience quality for saturated flow boiling in mini/micro-channels was developed by the authors of the present study [144] by considering various combinations of dimensional parameters, which include Weber number, We_{fo}, Capillary number, Ca, reduced pressure, P_R (= p/p_{crit}), density ratio, ρ_f/ρ_g, Boiling number, Bo, and ratio of the flow channel's heated to wetted perimeters, P_H/P_F. Table 7 provides a summary of this correlation whose empirical constants are optimized to yield least MAE versus the 997-point consolidated mini/microchannel database. The definitions of P_H, P_F and Boiling number for three-sided wall heating for a multi-channel heat sink with rectangular channels that is fitted atop with an insulating cover plate, and for a single circular channel with uniform circumferential wall heating are illustrated in Fig. 9(a) and (b), respectively. Fig. 10 shows the universal dryout incipience quality correlation predicts all three fluid subsets (refrigerants, CO_2, and water) of the consolidated database with good accuracy, evidenced by a MAE of 12.5%, with 93.6% and 98.0% of the data falling within ±30% and ±50% error bands, respectively.

The accuracy of the universal correlation is also examined in Table 8 by comparing individual mini/micro-channel databases from 26 sources with predictions of the universal correlation as well as select previous correlations that have shown relatively superior predictive capability. The universal correlation provides good predictions for all individual databases, with MAE values mostly within 20%, indicating that their accuracy is not compro-

Table 8
Comparison of individual mini/micro-channel dryout incipience databases with predictions of universal correlation for mini/micro-channels and select previous correlations [144].

Author(s)	D_h (mm)	Fluid(s)	Mean absolute error (%)				
			Wojtan et al. [125]	Del Col et al. [127]	Cheng et al. [128]	Mastrullo et al. [86]	Universal correlation
Becker [62]	2.4, 3.0	Water	96.3	24.2	69.0	10.2	19.8
Lezzi et al. [63]	1.0	Water	95.9	26.5	71.8	8.6	9.4
Baek and Chang [64]	6.0	Water	36.6	25.8	9.9	21.8	9.2
Roach et al. [65]	1.168, 1.448	Water	94.8	23.1	45.3	32.0	22.5
Kim et al. [66]	6.0	Water	29.1	28.5	8.7	24.2	7.2
Yang and Fujita [67]	0.976	R113	15.5	33.4	26.5	37.5	7.1
Yu et al. [68]	2.98	Water	30.8	33.2	25.4	31.7	19.6
Saitoh et al. [69]	0.51, 1.12, 3.1	R134a	23.1	17.9	26.0	29.2	22.1
Yun et al. [70]	1.14	CO_2	19.2	40.1	3.5	33.1	6.1
Hihara and Dang [71]	1.0, 2.0, 4.0, 6.0	CO_2	8.8	56.2	15.4	35.5	12.8
Greco [72]	6.0	R134a, R22, R407C, R410A	12.8	33.9	11.3	11.5	14.7
Shiferaw [73]	1.1, 2.88, 4.26	R134a	18.1	39.8	19.3	52.7	7.6
Ohta et al. [74]	0.51	FC72	17.9	16.4	20.9	32.5	25.2
Wang et al. [75]	1.3	R134a	19.1	3.5	13.3	13.0	16.6
Martín-Callizo [76]	0.64	R134a, R22, R245fa	29.4	24.9	25.9	61.3	16.5
Ali and Palm [77]	1.22, 1.70	R134a	40.5	38.1	31.1	54.1	22.0
Ducoulombier et al. [78]	0.529	CO_2	24.3	38.1	24.0	18.0	13.4
Oh and Son [79]	1.77, 3.36, 5.35	R134a, R22	5.6	10.6	12.2	6.5	11.1
Oh and Son [80]	4.57	CO_2	13.6	51.2	21.2	50.2	19.1
Oh et al. [81]	1.5, 3.0	R22, R410A, R290	19.1	29.6	12.8	33.4	13.5
Wu et al. [82]	1.42	CO_2	6.0	20.2	13.8	8.6	5.8
Del Col and Bortolin [83]	0.96	R134a, R245fa, R32	45.4	10.5	17.0	31.7	20.1
Karayiannis et al. [84]	1.1	R134a	9.7	22.7	15.8	38.7	9.5
Li et al. [85]	2.0	R1234yf, R32	8.5	5.8	5.2	14.2	8.8
Mastrullo et al. [86]	6.0	CO_2, R410A	2.0	40.5	14.2	2.1	5.2
Tibiriçá et al. [87]	1.0	R1234ze	32.6	10.3	22.7	5.6	25.7
Total			41.8	27.0	24.2	24.1	12.5

Table 9
Saturated flow boiling heat transfer data for mini/micro-channels included in the consolidated database [143].

Author(s)	Channel geometry[a]	Channel material	D_h (mm)	Relative roughness, e/D_h	Fluid(s)	G (kg/m^2 s)	Heat transfer characteristics[b]	Total data	Pre-dryout data[c]
Wambsganss et al. [88]	C single, H	Stainless steel	2.92	Smooth	R113	50–300	$h_{tp} = f(q'')$, NB	92	76
Tran [89]	C single, H	Brass	2.46	Smooth	R134a	33–502	$h_{tp} = f(q'')$, NB	302	302
Wang et al. [90]	C single, H	Copper	6.5	Smooth	R22	100–400	$h_{tp} = f(q'',G,x)$, NB + CB	63	61
Yan and Lin [91]	C multi, H	Copper	2.0	–	R134a	50–200	$h_{tp} = f(q'',G,x)$	137	116
Bao et al. [92]	C single, H	Copper	1.95	Smooth	R11, R123	167–560	$h_{tp} = f(q'')$, NB	164	143
Qu and Mudawar [93]	R multi, H	Copper + Lexan cover	0.349	–	Water	135–402	$h_{tp} = f(G,x)$, CB	335	335
Sumith et al. [94]	C single, VU	Stainless steel	1.45	–	Water	23–153	$h_{tp} = f(q'',G,x)$, CB	85	85
Yun et al. [95]	C single, H	Stainless steel	6.0	Smooth	R134a, CO_2	170–340	$h_{tp} = f(q'',G,x)$, NB	182	169
Huo et al. [96]	C single, VU	Stainless steel	2.01, 4.26	0.0009, 0.0004	R134a	100–500	$h_{tp} = f(q'',x)$, NB	365	323
Lee and Mudawar [97]	R multi, H	Copper + Lexan cover	0.349	–	R134a	61–657	$h_{tp} = f(q'',x)$, NB + CB	111	63
Saitoh et al. [69]	C single, H	Stainless steel	0.51, 1.12, 3.1	Smooth	R134a	150, 300	$h_{tp} = f(q'',G,x)$, NB + CB	420	259
Yun et al. [70]	R multi, H	Stainless steel	1.14, 1.53, 1.54	-	CO_2	200–400	$h_{tp} = f(q'',x)$, NB	57	43
Muwanga and Hassan [98]	C single, H	Stainless steel	1.067	–	FC72	770–1040	$h_{tp} = f(q'',G)$	454	327
Zhao and Bansal [99]	C single, H	Stainless steel	4.57	Smooth	CO_2	140–231	$h_{tp} = f(q'',G,x)$	22	19
Agostini et al. [100]	R multi, H	Silicon + Lexan cover	0.336	0.0005	R236fa	281–1370	$h_{tp} = f(q'',x)$, NB	593	458
Consolini [101]	C single, H	Stainless steel	0.51, 0.79	0.0047, 0.0022	R134a, R236fa, R245fa	274–1435	$h_{tp} = f(q'', x)$	650	585
Greco [72]	C single, H	Stainless steel	6.0	Smooth	R134a, R22, R404A, R407C, R410A, R417A	199–1100	$h_{tp} = f(q'',G, x)$, NB + CB	516	491
Bertsch et al. [102]	R multi, H	Copper + Lexan cover	0.544, 1.089	< 0.0009, < 0.0006	R134a, R245fa	19–336	$h_{tp} = f(q'',x)$, NB	332	214
In and Jeong [103]	C single, H	Stainless steel	0.19	–	R123, R134a	314–470	$h_{tp} = f(q'',G,x)$, NB + CB	256	159
Mastrullo et al. [104]	C single, H	Stainless steel	6.0	Smooth	CO_2	200–349	$h_{tp} = f(q'',x)$, NB	143	135
Ohta et al. [74]	C single, H	Stainless steel	0.51	–	FC72	107, 215	–	24	13
Wang et al. [75]	C single, H	Stainless steel	1.3	–	R134a	321–836	$h_{tp} = f(q'',x)$, NB	365	322
Ducoulombier [105]	C single, H	Stainless steel	0.529	0.0015–0.0030	CO_2	200–1400	$h_{tp} = f(q'',G,x)$, NB + CB	1573	1080
Hamdar et al. [106]	R single, H	Aluminum	1.0	–	R152a	210–580	$h_{tp} = f(q'')$, NB	50	45
Martín-Callizo [76]	C single, VU	Stainless steel	0.64	0.0012	R134a, R22	185–535	$h_{tp} = f(q'',x)$	381	335
Ong [107]	C single, H	Stainless steel	1.03, 2.20, 3.04,	0.0006, 0.0004, 0.0003	R134a, R236fa, R245fa,	199–1608	$h_{tp} = f(q'',G,x)$, NB + CB	2504	2247
Tibiriçá and Ribatski [108]	C single, H	Stainless steel	2.32	0.0001	R134a, R245fa	50–700	$h_{tp} = f(q'',G, x)$, NB + CB	130	96
Ali et al. [109]	C single, VU	Stainless steel	1.7	0.0001	R134a	75–600	$h_{tp} = f(q'',x)$, NB	152	136
Bang et al. [110]	C single, H	Stainless steel	1.73	–	Water	100	$h_{tp} = f(x)$, CB	65	65
Copetti et al. [111]	C single, H	Stainless steel	2.62	0.0008	R134a	240–932	$h_{tp} = f(q'',G,x)$	876	845
Mahmoud et al. [112]	C single, VU	Stainless steel	1.1	0.0012	R134a	128–549	$h_{tp} = f(q'')$, NB	152	134
Oh and Son [79]	C single, H	Copper	1.77, 3.36, 5.35	Smooth	R134a, R22	200–500	$h_{tp} = f(G,x)$, CB	153	131
Oh and Son [80]	C single, H	Stainless steel	4.57	Smooth	CO_2	400–900	$h_{tp} = f(q'',x)$, NB	107	62
Wu et al. [82]	C single, H	Stainless steel	1.42	-	CO_2	300–600	$h_{tp} = f(q'',G,x)$, NB + CB	419	297
Karayiannis et al. [84]	C single, VU	Stainless steel	1.1	0.0012	R134a	215–550	$h_{tp} = f(q'',G,x)$, NB	545	489
Li et al. [85]	C single, H	Stainless steel	2.0	Smooth	R1234yf, R32	100–400	$h_{tp} = f(q'',G,x)$, NB + CB	169	134
Tibiriçá et al. [87]	C single, H	Stainless steel	1.0, 2.2	0.0006, 0.0004	R1234ze	300–600	$h_{tp} = f(G,x)$	30	11
Total								12,974	10,805

[a] C: circular, R: rectangular, H: horizontal, VU: vertical upflow.
[b] NB: nucleate boiling dominant data as designated by original authors, CB: convective boiling dominant data as designated by original authors.
[c] Pre-dryout data corresponding to $x < x_{di}$ based on Table 7.

Table 10
Previous saturated flow boiling heat transfer correlations,[a] and their predictions to 10,805 pre-dryout data points for mini/micro-channel flows [143].

Author(s)	Equation	Remarks	MAE[b] (%)	θ (%)	ξ (%)
Recommended for macro-channels					
Shah [130]	$h_{tp} = max(E,S)h_{sp},\ h_{sp} = 0.023Re_f^{0.8}Pr_f^{0.4}\frac{k_f}{D_h}$, for $N > 1.0$, $S = 1.8/N^{0.8}$, $E = 230Bo^{0.5}$ for $Bo > 3\times10^{-5}$, or $E = 1 + 46Bo^{0.5}$ for $Bo < 3\times10^{-5}$, for $0.1 < N \leqslant 1.0$, $S = 1.8/N^{0.8}$, $E = F\,Bo^{0.5}\exp(2.74N^{-0.1})$, for $N \leqslant 0.1$, $S = 1.8/N^{0.8}$, $E = F\,Bo^{0.5}\exp(2.47N^{-0.15})$, $F = 14.7$ for $Bo \geqslant 11\times10^{-4}$, or $F = 15.43$ for $Bo < 11\times10^{-4}$, $N = Co$ for vertical tube, $N = Co$ for horizontal tube with $Fr_f \geqslant 0.04$, $N = 0.38Fr_f^{-0.3}Co$ for horizontal tube with $Fr_f < 0.04$, $Re_f = \frac{G(1-x)D_h}{\mu_f},\ Co = \left(\frac{1-x}{x}\right)^{0.8}\left(\frac{\rho_g}{\rho_f}\right)^{0.5},\ Fr_f = \frac{G^2}{\rho_f^2 gD_h}$	D = 6–25.4 mm, water, R11, R12, R22, R113, cyclohexane, 780 data points	32.0	57.0	85.7
Cooper [131]	$h_{tp} = 55P_R^{0.12}(-\log_{10}P_R)^{-0.55}M^{-0.5}q_H''^{0.67}$	6000 data points for nucleate pool boiling	33.2	46.2	83.1
Gungor and Winterton [132]	$h_{tp} = Eh_{sp} + Sh_{nb},\ h_{sp} = 0.023Re_f^{0.8}Pr_f^{0.4}\frac{k_f}{D_h},\ E = 1 + 24000Bo^{1.16} + 1.37\left(\frac{1}{X_{tt}}\right)^{0.86},\ h_{nb} = h_{tp,Cooper},\ S = \left(1 + 1.15\times10^{-6}E^2Re_f^{1.17}\right)^{-1}$, for horizontal tube with $Fr_f \leqslant 0.05$, replace E and S with $EFr_f^{(0.1-2Fr_f)}$ and $SFr_f^{0.5}$, respectively	D = 2.95–32.0 mm, water, R11, R12, R113, R114, R22, ethylene glycol, 4300 data points	55.9	41.6	59.3
Liu and Winterton [133]	$h_{tp} = \left[(Eh_{sp})^2 + (Sh_{nb})^2\right]^{0.5}, h_{sp} = 0.023Re_{fo}^{0.8}Pr_f^{0.4}\frac{k_f}{D_h}, E = \left[1 + xPr_f\left(\frac{\rho_f}{\rho_g} - 1\right)\right]^{0.35}, h_{nb} = h_{tp,Cooper},\ S = \left(1 + 0.055E^{0.1}Re_{fo}^{0.16}\right)^{-1}$, for horizontal tube with $Fr_f \leqslant 0.05$, replace E and S with $EFr_f^{(0.1-2Fr_f)}$ and $SFr_f^{0.5}$, respectively	Same data as Gungor and Winterton's [132]	28.1	63.4	90.4
Recommended for mini/micro-channels					
Lazarek and Black [134]	$h_{tp} = \left(30Re_{fo}^{0.857}Bo^{0.714}\right)\left(\frac{k_f}{D_h}\right), Re_{fo} = \frac{GD_h}{\mu_f},\ Bo = \frac{q_H''}{Gh_{fg}}$	D = 3.15 mm, R113, nucleate boiling dominant	28.2	61.6	87.4
Tran et al. [6]	$h_{tp} = 8.4\times10^5\left(Bo^2We_{fo}\right)^{0.3}\left(\frac{\rho_g}{\rho_f}\right)^{0.4},\ We_{fo} = \frac{G^2D_h}{\rho_f\sigma}$	D = 2.46,2.92 mm, D_h = 2.40 mm, R12, R113, nucleate boiling dominant	41.1	41.1	63.7
Warrier et al. [135]	$h_{tp} = Eh_{sp},\ h_{sp} = 0.023Re_{fo}^{0.8}Pr_f^{0.4}\frac{k_f}{D_h},\ E = 1.0 + 6.0Bo^{1/16} - 5.3(1 - 855Bo)x^{0.65}$	D_h = 0.75 mm, five parallel, FC84	46.2	32.1	60.0
Yu et al. [68]	$h_{tp} = 6.4\times10^6\left(Bo^2We_{fo}\right)^{0.27}\left(\frac{\rho_g}{\rho_f}\right)^{0.2}$	D = 2.98 mm, water, ethylene glycol, nucleate boiling dominant	–	1.9	3.6
Agostini and Bontemps [136]	$h_{tp} = 28q_H''^{2/3}G^{-0.26}x^{-0.10}$ for $x < 0.43$, $h_{tp} = 28q_H''^{2/3}G^{-0.64}x^{-2.08}$ for $x > 0.43$	D_h = 2.01 mm, 11 parallel, R134a	54.7	38.4	55.9
Bertsch et al. [137]	$h_{tp} = Eh_{cb} + Sh_{nb},\ h_{cb} = h_{sp,fo}(1-x) + h_{sp,go}x,\ E = 1 + 80(x^2 - x^6)\exp(-0.6N_{conf}),\ h_{nb} = h_{tp,Cooper},\ S = 1 - x,$ $N_{conf} = \sqrt{\frac{\sigma}{g(\rho_f-\rho_g)D_h^2}},\ h_{sp,fo} = \left(3.66 + \frac{0.0668\frac{D_h}{L}Re_{fo}Pr_f}{1+0.04\left[\frac{D_h}{L}Re_{fo}Pr_f\right]^{2/3}}\right)\frac{k_f}{D_h}, h_{sp,go} = \left(3.66 + \frac{0.0668\frac{D_h}{L}Re_{go}Pr_g}{1+0.04\left[\frac{D_h}{L}Re_{go}Pr_g\right]^{2/3}}\right)\frac{k_g}{D_h},\ Re_{fo} = \frac{GD_h}{\mu_f},\ Re_{go} = \frac{GD_h}{\mu_g}$	D_h = 0.16–2.92 mm, water, refrigerants, FC-77, nitrogen, 3899 data points	30.5	51.1	88.7
Li and Wu [138]	$h_{tp} = 334Bo^{0.3}\left(BdRe_f^{0.36}\right)^{0.4}\frac{k_f}{D_h},\ Bd = \frac{g(\rho_f-\rho_g)D_h^2}{\sigma}$	D_h = 0.16–3.1 mm, water, refrigerants, FC-77, ethanol, propane, CO_2, 3744 data points	50.6	49.9	67.6
Ducoulombier et al. [78]	$h_{tp} = max(h_{nb}, h_{cb}),\ h_{nb} = 131P_R^{-0.0063}(-\log_{10}P_R)^{-0.55}M^{-0.5}q_H''^{0.58}$, if $Bo > 1.1\times10^{-4}$, $h_{cb} = \left[1.47\times10^4Bo + 0.93\left(\frac{1}{X_{tt}}\right)^{2/3}\right]\left(0.023Re_{fo}^{0.8}Pr_f^{1/3}\frac{k_f}{D_h}\right)$, if $Bo < 1.1\times10^{-4}$, $h_{cb} = \left[1 + 1.80\left(\frac{1}{X_{tt}}\right)^{0.986}\right]\left(0.023Re_f^{0.8}Pr_f^{0.4}\frac{k_f}{D_h}\right)$	D = 0.529 mm, CO_2	59.4	44.0	59.3
Oh and Son [79]	$h_{tp} = 0.034Re_f^{0.8}Pr_f^{0.3}\left[1.58\left(\frac{1}{X_{tt}}\right)^{0.87}\right]\left(\frac{k_f}{D_h}\right)$	D = 1.77, 3.36, 5.35 mm, R134a, R22	55.5	20.9	40.2

[a] The Cooper [131] correlation was developed for nucleate pool boiling.
[b] Dash indicates mean absolute error $\gg$ 100%.

Table 11
Universal correlation for pre-dryout saturated flow boiling heat transfer in mini/micro-channels in both single- and multi-channel configurations [143].

$$h_{tp} = \left(h_{nb}^2 + h_{cb}^2\right)^{0.5}$$

$$h_{nb} = \left[2345\left(Bo\frac{P_H}{P_F}\right)^{0.70} P_R^{0.38}(1-x)^{-0.51}\right]\left(0.023Re_f^{0.8}Pr_f^{0.4}\frac{k_f}{D_h}\right)$$

$$h_{cb} = \left[5.2\left(Bo\frac{P_H}{P_F}\right)^{0.08} We_{fo}^{-0.54} + 3.5\left(\frac{1}{X_{tt}}\right)^{0.94}\left(\frac{\rho_g}{\rho_f}\right)^{0.25}\right]\left(0.023Re_f^{0.8}Pr_f^{0.4}\frac{k_f}{D_h}\right)$$

where $Bo = \frac{q''_H}{Gh_{fg}}$, $P_R = \frac{p}{p_{crit}}$, $Re_f = \frac{G(1-x)D_h}{\mu_f}$, $We_{fo} = \frac{G^2 D_h}{\rho_f \sigma}$, $X_{tt} = \left(\frac{\mu_f}{\mu_g}\right)^{0.1}\left(\frac{1-x}{x}\right)^{0.9}\left(\frac{\rho_g}{\rho_f}\right)^{0.5}$: effective heat flux averaged over heated perimeter of channel, P_H: heated perimeter of channel, P_F: wetted perimeter of channel

Correlation based on consolidated database of 10,805 saturated boiling heat transfer coefficient data points from 37 sources with the following application range:

- Working fluid: FC72, R11, R113, R123, R1234yf, R1234ze, R134a, R152a, R22, R236fa, R245fa, R32, R404A, R407C, R410A, R417A, CO_2, and water
- Hydraulic diameter: $0.19 < D_h < 6.5$ mm
- Mass velocity: $19 < G < 1608$ kg/m^2 s
- Liquid-only Reynolds number: $57 < Re_{fo} = GD_h/\mu_f < 49,820$
- Flow quality: $0 < x < 1$
- Reduced pressure: $0.005 < P_R < 0.69$

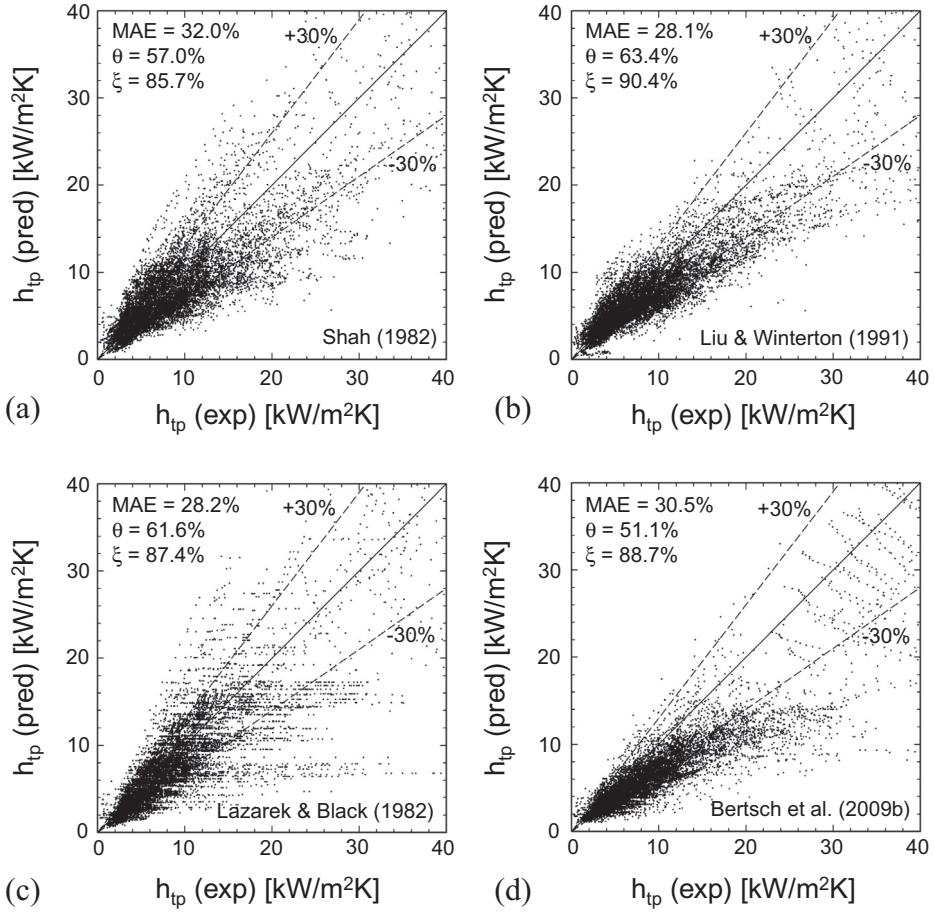

Fig. 11. Comparison of 10,805 point consolidated database for pre-dryout saturated flow boiling heat transfer in mini/micro-channels with predictions of correlations of (a) Shah [130], (b) Liu and Winterton [133], (c) Lazarek and Black [134], and (d) Bertsch et al. [137] (adapted from [143]).

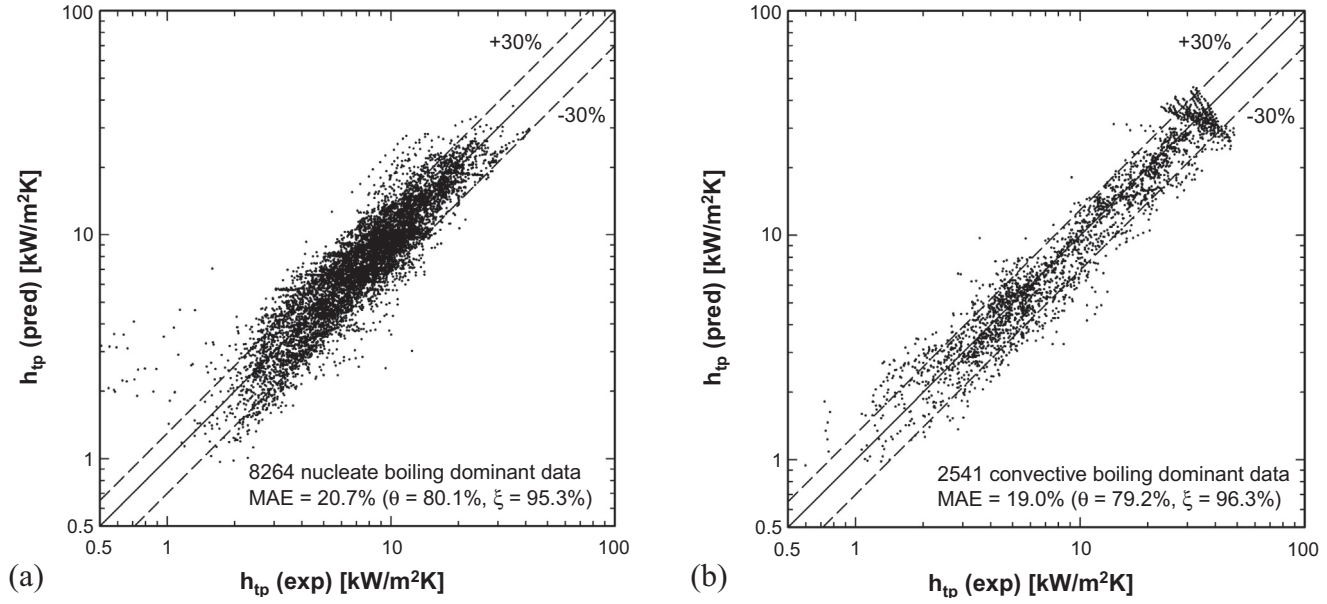

Fig. 12. Comparison of predictions of universal saturated flow boiling heat transfer correlation with two subsets of 10,805 point pre-dryout database corresponding to (a) nucleate boiling dominant data and (b) convective boiling dominant data. Nucleate boiling dominant data correspond to $h_{nb}/h_{cb} > 1.0$, where h_{nb} and h_{cb} are calculated using Table 11 (adapted from [143]).

mised against specific databases. With the most superior MAE of 12.5%, the universal correlation predicts 11 databases more accurately than by any of the select previous correlations.

5. Heat transfer in flow boiling

5.1. Consolidation of world databases for flow boiling in mini/micro-channels

A total of 12,974 data points for flow boiling heat transfer in mini/micro-channels were amassed by the present authors [143] from 37 sources [69,70,72,74–76,79,80,82,84,85,87–112]. Table 9 describes the individual databases comprising the consolidated database, which includes 11,409 single-channel data points from 31 sources, and 1565 multi-channel data points from 6 sources. To develop a universal correlation for the pre-dryout heat transfer coefficient associated with saturated flow boiling, any partial dryout or post-dryout data are identified using the universal dryout incipience quality correlation, Table 7, and excluded from the consolidated database. The remaining 10,805 pre-dryout data points consist of 9576 single-channel and 1229 multi-channel data points. Table 9 provides key information on the 37 individual databases including the dependence of heat flux, mass velocity, and quality on the two-phase heat transfer coefficient, as well as the dominant heat transfer mechanism as suggested by the original authors. The consolidated database covers a wide range of working fluids and geometrical and flow parameters, as presented later.

5.2. Assessment of previous boiling heat transfer correlations against consolidated database for flow boiling in mini/micro-channels

Table 10 provides a summary of previous saturated flow boiling heat transfer correlations that have been recommended for macro-channels [130–133] and mini/micro-channels [6,68,78,79,134–138]. Applicable range of channel diameter and working fluids for each correlation are also indicated in Table 10. In an effort to develop a generalized correlation for saturated flow boiling, Shah [130], Gungor and Winterton [132] and Liu and Winterton [133] proposed correlations based on fairly large databases for macro-channels, and Bertsch et al. [137] and Li and Wu [138] for mini/micro-channels. Notice that the Cooper [131] correlation has been recommended for nucleate flow boiling in several published works, such as those of Gungor and Winterton [132], Liu and Winterton [133], Bao et al. [92], Yun et al. [70] and Bertsch et al. [102,137], was originally developed for nucleate pool boiling. Since the correlations in Table 10 are intended for uniform circumferential heating in circular tubes or rectangular channels with four-sided heating, the multiplier used for three-sided wall cooling, Eq. (1), is also adopted when applying these correlations to rectangular channels with three-sided wall heating, such as the data of Qu and Mudawar [93], Lee and Mudawar [97], Agostini et al. [100] and Bertsch et al. [102]. Table 10 compares the 10,805 pre-dryout data points with predictions of previous empirical heat transfer correlations, where the MAE is calculated according to Eq. (4). Among all previous correlations, those of Liu and Winterton and Lazarek and Black show relatively fair predictions, with MAE values of 28.1%, and 28.2%, respectively.

Fig. 11(a)–(d) compare the 10,805 pre-dryout data points for mini/micro-channels with predictions of select previous heat transfer correlations that have shown relatively superior predictive capability. A large fraction of the database is underpredicted by the correlations of Lazarek and Black [134] and Bertsch et al. [137]. Most of the high pressure data are underpredicted by the correlations of Shah [130] and Liu and Winterton [133], while most of the high pressure data are overpredicted by the correlation of Lazarek and Black.

5.3. Universal predictive method based on consolidated database for flow boiling in mini/micro-channels

A universal method to predicting the two-phase heat transfer coefficient for saturated flow boiling in mini/micro-channels was developed by the authors [143] based on the following popular functional form of Schrock and Grossman [154],

Table 12
Comparison of individual mini/micro-channel pre-dryout heat transfer databases with predictions of universal correlation for mini/micro-channels and select previous correlations [143].

Author(s)	D_h (mm)	Fluid(s)	$(h_{nb}/h_{cb})_{avg}$[a]	Mean absolute error (%)				
				Shah [130]	Liu and Winterton [133]	Lazarek and Black [134]	Bertsch et al. [137]	Universal correlation
Wambsganss et al. [88]	2.92	R113	2.12	21.6	27.2	20.0	19.6	25.5
Tran [89]	2.46	R134a	1.71	30.8	27.5	31.5	31.0	23.1
Wang et al. [90]	6.5	R22	0.65	33.2	33.6	26.5	27.9	26.2
Yan and Lin [91]	2.0	R134a	1.44	31.0	23.7	35.9	24.2	21.8
Bao et al. [92]	1.95	R11, R123	5.24	18.6	28.8	9.6	29.6	14.2
Qu and Mudawar [93]	0.349	Water	0.26	61.8	41.8	41.0	19.5	20.5
Sumith et al. [94]	1.45	Water	0.21	35.3	31.1	36.4	40.2	28.6
Yun et al. [95]	6.0	R134a, CO_2	2.37	39.8	23.9	33.1	24.4	24.0
Huo et al. [96]	2.01, 4.26	R134a	7.92	34.3	28.1	16.0	25.6	13.6
Lee and Mudawar [97]	0.349	R134a	2.93	21.7	41.5	12.6	46.9	26.2
Saitoh et al. [69]	0.51, 1.12, 3.1	R134a	0.72	17.3	19.6	30.7	31.1	14.4
Yun et al. [70]	1.14, 1.53, 1.54	CO_2	2.00	45.4	20.9	26.7	24.0	18.6
Muwanga and Hassan [98]	1.067	FC72	6.80	40.4	30.9	19.2	42.7	22.4
Zhao and Bansal [99]	4.57	CO_2	1.16	15.7	14.6	12.4	26.6	10.2
Agostini et al. [100]	0.336	R236fa	3.35	52.1	36.9	34.4	25.1	17.8
Consolini [101]	0.51, 0.79	R134a, R236fa, R245fa	3.55	30.7	32.5	14.9	33.1	14.9
Greco [72]	6.0	R134a, R22, R404A, R407C, R410A, R417A	1.00	41.1	50.2	28.5	36.5	21.0
Bertsch et al. [102]	0.544, 1.089	R134a, R245fa	3.34	24.0	26.4	46.3	22.4	22.0
In and Jeong [103]	0.19	R123, R134a	0.77	32.3	42.6	40.9	45.8	13.0
Mastrullo et al. [104]	6.0	CO_2	2.08	34.9	14.0	19.9	13.3	15.5
Ohta et al. [74]	0.51	FC72	1.14	29.2	17.6	27.0	21.3	11.0
Wang et al. [75]	1.3	R134a	2.65	23.3	26.8	24.6	44.3	17.2
Ducoulombier [105]	0.529	CO_2	1.34	29.1	23.9	37.5	38.3	15.9
Hamdar et al. [106]	1.0	R152a	1.11	29.0	22.7	39.5	46.7	29.6
Martín-Callizo [76]	0.64	R134a, R22	2.91	9.3	15.8	15.3	23.1	19.8
Ong [107]	1.03, 2.20, 3.04,	R134a, R236fa, R245fa,	3.64	33.9	23.8	25.3	21.9	24.7
Tibiriçá and Ribatski [108]	2.32	R134a, R245fa	0.91	13.6	15.5	37.2	31.3	17.8
Ali et al. [109]	1.7	R134a	4.79	39.5	34.2	29.6	31.8	28.7
Bang et al. [110]	1.73	Water	0.36	31.4	20.1	29.8	25.2	15.1
Copetti et al. [111]	2.62	R134a	3.18	19.2	21.0	25.0	29.2	19.8
Mahmoud et al. [112]	1.1	R134a	4.94	36.5	41.9	23.2	40.3	16.7
Oh and Son [79]	1.77, 3.36, 5.35	R134a, R22	1.52	26.6	25.1	33.3	37.4	21.8
Oh and Son [80]	4.57	CO_2	10.00	36.5	7.1	12.4	22.0	18.4
Wu et al. [82]	1.42	CO_2	1.42	34.6	25.0	41.3	30.8	16.4
Karayiannis et al. [84]	1.1	R134a	3.20	36.9	43.0	31.1	47.0	28.2
Li et al. [85]	2.0	R1234yf, R32	0.73	21.9	19.5	40.2	42.6	14.5
Tibiriçá et al. [87]	1.0, 2.2	R1234ze	1.82	14.7	11.7	10.0	19.5	19.8
Total				32.0	28.1	28.2	30.5	20.3

[a] Average value of h_{nb}/h_{cb} for individual database, where h_{nb} and h_{cb} are calculated using Table 11.

$$h_{tp} = \left[C_1 Bo + C_2 \left(\frac{1}{X_{tt}}\right)^{2/3}\right]\left(0.023 Re_{fo}^{0.8} Pr_f^{0.4} \frac{k_f}{D_h}\right), \quad (10)$$

where the first and second terms in the first multiplier reflect the influences of the nucleate boiling dominant and convective boiling dominant regimes, respectively, and the second multiplier is the Dittus–Boetler single-phase heat transfer coefficient relation based on Re_{fo}. Two different relations of h_{nb} and h_{cb} are proposed to predict the heat transfer coefficient for the nucleate boiling dominant regime and the convective boiling dominant regime, respectively. Each relation modifies the general functional form of Schrock and Grossman by incorporating the nucleate boiling suppression term, $(1-x)^{-N}$, Weber number, We_{fo}, reduced pressure, P_R (=p/p_{crit}), density ratio, ρ_f/ρ_g, and ratio of the flow channel's heated to wetted perimeters, P_H/P_F, as well as by replacing Re_{fo} in the Dittus–Boetler relation with Re_f. Superpositioning the contributions of nucleate boiling, h_{nb}, and convective boiling, h_{cb}, is used to obtain a single relation for the heat transfer coefficient. The universal correlation for saturated flow boiling in mini/micro-channels is summarized in Table 11, where empirical constants are determined by minimizing MAE against the 10,805 point pre-dryout database. Note that, to tackle three-sided wall heating in flow boiling, the ratio of the flow channel's heated to wetted

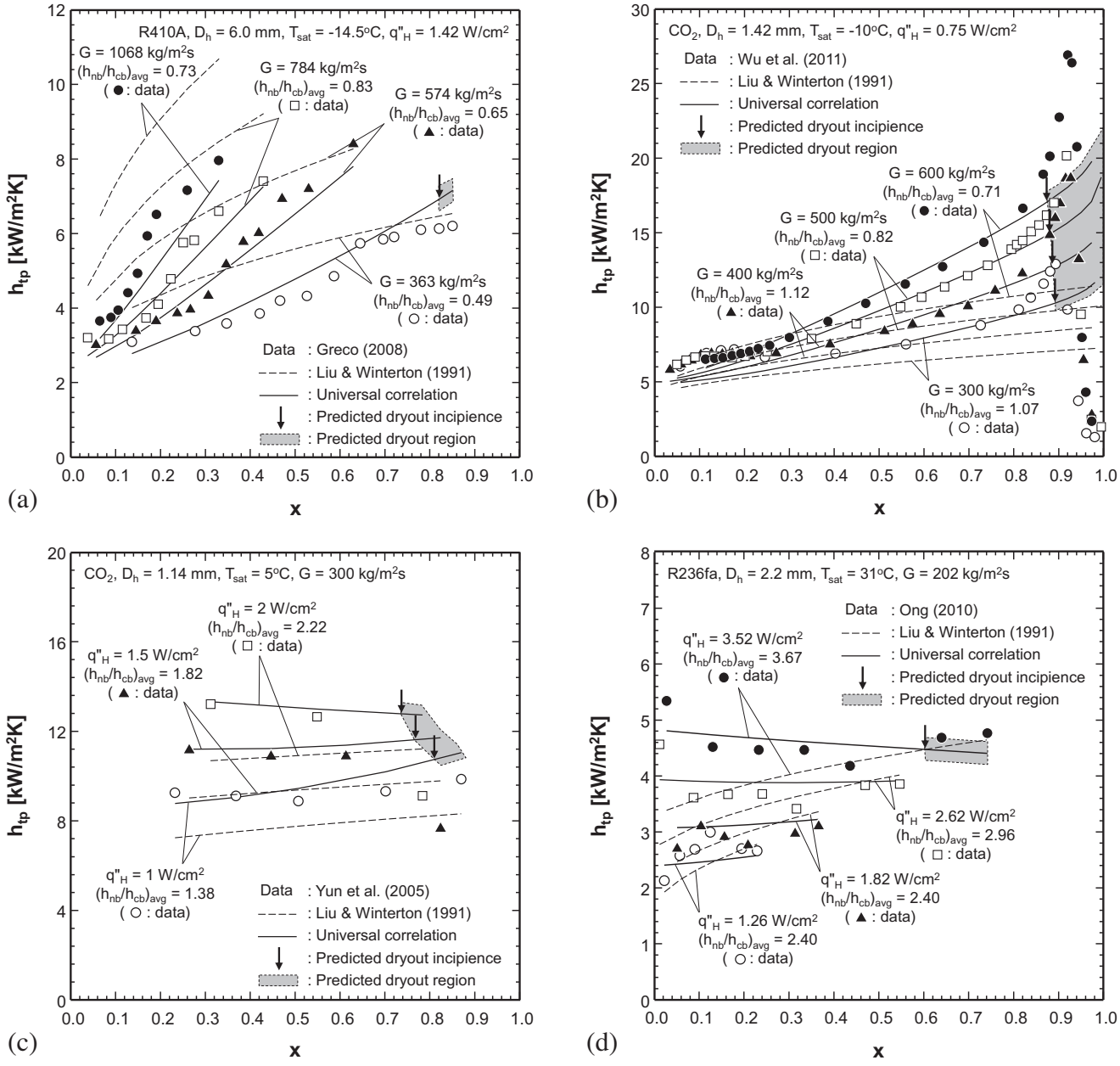

Fig. 13. Comparison of predictions of universal saturated flow boiling heat transfer correlation [143] and Liu and Winterton's [133] correlation with experimental data for convective boiling dominant heat transfer by (a) Greco [72] and (b) Wu et al. [82], and nucleate boiling dominant heat transfer by (c) Yun et al. [70] and (d) Ong [107] (adapted from [143]).

perimeters, P_H/P_F, and Boiling number based on effective heat flux averaged over the heated perimeter, q''_H, are used, instead of using the multiplier for three-sided wall cooling in flow condensation, which is given by Eq. (1) and provided in Table 3. The definitions of P_H, P_F and Boiling number for rectangular multi-channels with three-sided wall heating, and for a single circular channel with uniform circumferential wall heating are illustrated in Fig. 9(a) and (b), respectively. Fig. 12(a) and (b) show the universal local heat transfer coefficient correlation predicts two subsets of the 10,805 point pre-dryout database consisting of 8264 nucleate boiling dominant data points and 2541 convective boiling dominant data points with good accuracy, evidenced by MAEs of 20.7%, and 19.0%, respectively.

Table 12 compares individual mini/micro-channel pre-dryout heat transfer databases from 37 sources with predictions of the universal correlation as well as select previous correlations that have shown relatively superior predictive capability. The dominant heat transfer mechanism for individual databases can be determined by the average value of h_{nb}/h_{cb} presented in Table 12. A higher value of $(h_{nb}/h_{cb})_{avg}$ indicates nucleate boiling is more dominant, whereas a lower value indicates convective boiling is more dominant. Notice that the previous correlations are incapable of providing evenly good predictions for all individual databases. The correlations of Shah [130], Liu and Winterton [133], and Lazarek and Black [134] provide inferior predictions for very small diameters below 0.5 mm. Most of the convective boiling dominant data are predicted with poor accuracy by Lazarek and Black [134] and Bertsch et al. [137]. In contrast, the universal correlation provides very good predictions for all individual databases, with 23 databases predicted more accurately than any of the select previous correlations, and with the best overall MAE of 20.3%.

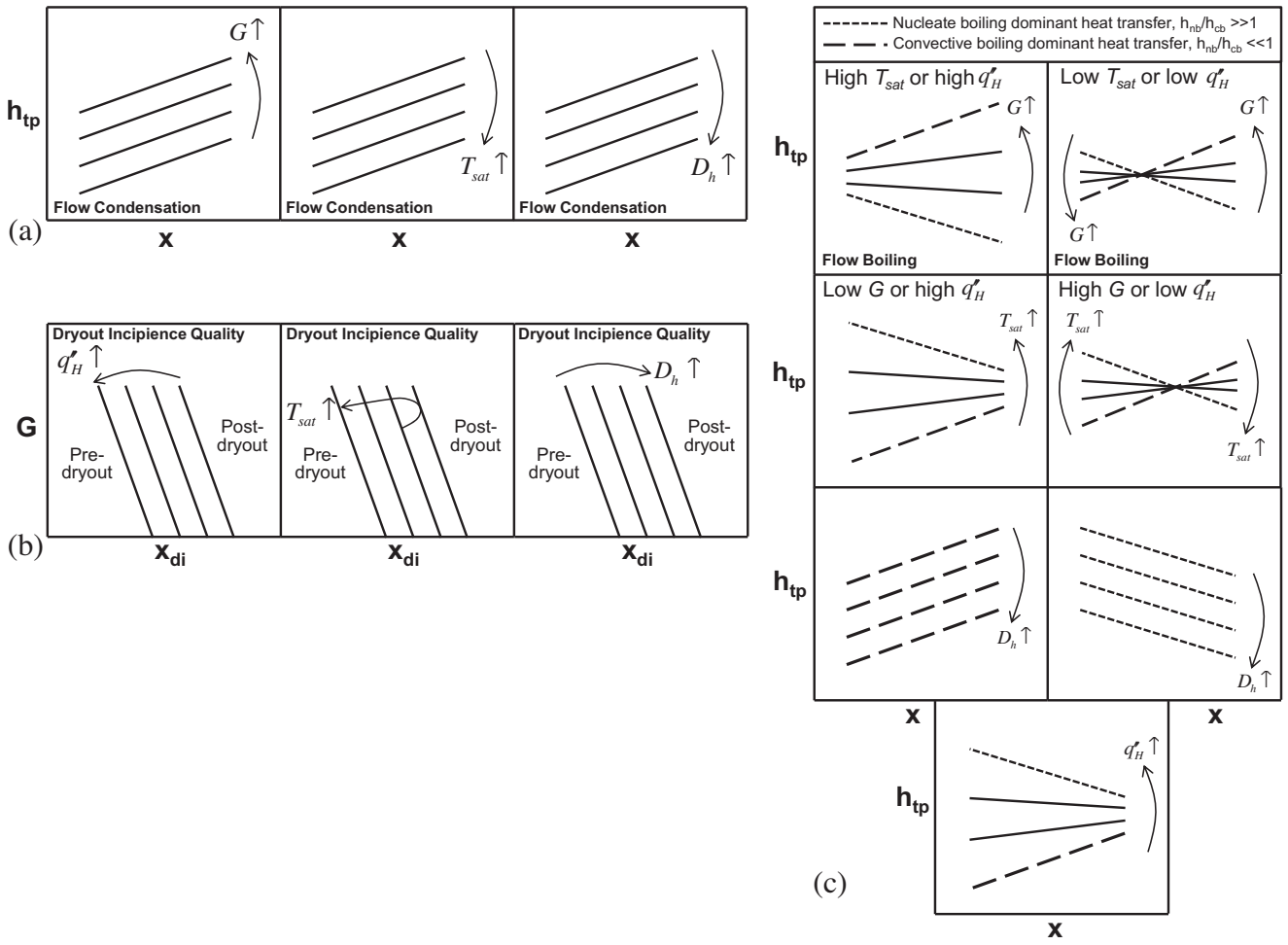

Fig. 14. Schematic representation of parametric trends according to universal predictive methods. (a) Condensation heat transfer coefficient versus quality for different G, T_{sat} and D_h. (b) Mass velocity versus dryout incipience quality for different q''_H, T_{sat} and D_h. (c) Boiling heat transfer coefficient versus quality for different G, T_{sat}, D_h and q''_H.

Predictions of the universal correlation and Liu and Winterton [133] correlation are compared with representative convective boiling dominant data [72,82] and nucleate boiling dominant data [70,107] in Fig. 13(a)–(d), respectively. These figures show that the universal local heat transfer correlation accurately captures experimental data in both magnitude and trend. For the convective boiling dominant data corresponding to low $(h_{nb}/h_{cb})_{avg}$ values, Fig. 13(a) and (b), the heat transfer coefficient has a positive slope versus quality, and increases with increasing mass velocity in both data and predictions. Notice that the locations of dryout incipience, where the heat transfer coefficient begins to decrease appreciably, are predicted with good accuracy by the universal dryout incipience quality correlation in Table 7. For the nucleate boiling dominant data corresponding to high $(h_{nb}/h_{cb})_{avg}$ values, Fig. 13(c) and (d), the heat transfer coefficient increases with increasing heat flux, and the slope of h_{tp} versus x becomes negative with increasing heat flux.

Fig. 14(a)–(c) present the complex parametric trends predicted by the universal correlations for the condensation heat transfer coefficient, dryout incipience quality, and boiling heat transfer coefficient, which are summarized in Tables 3, 7, and 11, respectively. Fig. 14(a) shows the condensation heat transfer coefficient, h_{tp}, has a positive slope versus quality, x, increases with increasing mass velocity, G, and decreases with increasing saturation temperature, T_{sat}, or channel diameter, D_h. Fig. 14(b) shows for the dryout incipience quality, G versus x_{di} generally has a negative slope, but could have a positive slope for relatively low q''_H or low T_{sat} [144]. Increasing q''_H or decreasing D decreases x_{di}. x_{di} increases with increasing T_{sat} up to a certain point then decreases with increasing T_{sat}. Fig. 14(c) shows the variation of the boiling heat transfer coefficient with x changes depending on the dominant heat transfer regime. h_{tp} versus x has a negative slope for the nucleate boiling dominant heat transfer regime where $h_{nb}/h_{cb} \gg 1$, and a positive slope for the convective boiling dominant heat transfer regime where $h_{nb}/h_{cb} \ll 1$. The contribution of convective boiling increases with increasing G, resulting in the slope of h_{tp} versus x changing from negative to positive. Notice that with decreasing T_{sat} or q''_H, the low x region where h_{tp} decreases with increasing G is extended. The contribution of nucleate boiling increases with increasing T_{sat} or q''_H. h_{tp} decreases with increasing D_h for both boiling heat transfer regimes.

Looking ahead, the success of the universal predictive tools should help pave the way for a shift in research efforts from empirical formulation to both theoretical and computational models for both condensing and boiling mini/micro-channel flows. Such models must be able to tackle the complex interfacial interactions specific to small diameter channels. In addition, models must be able to both predict transitions between flow regimes and capture the underlying physics for each regime. Most importantly, models for the annular regime must address the important influences of interfacial waves. Past studies at PU-BTPFL involving adiabatic, heated and evaporating liquid films have shown that waves can have a profound influence on mass, momentum and heat transfer [155–160]. These modeling efforts can also benefit greatly from the use of

sophisticated diagnostic techniques for measurement of film thickness and interfacial waves [157–161], albeit for small channel diameters.

6. Conclusions

This study reviewed methods for predicting heat transfer in condensing and boiling mini/micro-channel flows. Previous methods were assessed for accuracy in predicting flow condensing and boiling data, which required consolidation of world databases for each heat transfer category. Key findings from the study are as follows:

1. Three separate consolidated mini/micro-channel databases are discussed. The first is for flow condensation heat transfer, and includes 4045 data points from 28 sources. The second is for dryout incipience quality, and includes 997 data points from 26 sources. The third database is for saturated boiling heat transfer and includes 10,805 data points from 37 sources. These databases cover numerous working fluids, and broad ranges of geometrical and flow parameters.
2. Previous correlations for condensation heat transfer, dryout incipience quality, and saturated boiling heat transfer in both mini/micro-channels and macro-channels are carefully assessed. It is shown that despite their success in predicting heat transfer for specific fluids and narrow databases, they are unable to provide accurate predictions against entire consolidated databases.
3. Three separate universal predictive methods are discussed whose development is rooted in minimizing MAE against the consolidated databases. The universal method for predicting condensation heat transfer consists of two separate correlations, one for annular flow, and the second for slug and bubbly flows. To develop a correlation for pre-dryout saturated flow boiling heat transfer, partial dryout and post-dryout data are first segregated using a universal correlation for dryout incipience quality. The universal method for predicting saturated boiling heat transfer is able to tackle both nucleate boiling dominated and convective boiling dominated regimes up to the location of incipient dryout. All three universal predictive methods are proven capable of predicting the consolidated databases in both trend and magnitude with high accuracy.

Conflict of interest

None declared.

Acknowledgment

The authors are grateful for the support for this project from the National Aeronautics and Space Administration (NASA) under Grant No. NNX13AC83G.

References

[1] I. Mudawar, Assessment of high-heat-flux thermal management schemes, IEEE Trans. CPMT: Compon. Packag. Technol. 24 (2001) 122–141.
[2] I. Mudawar, Two-phase micro-channel heat sinks: theory, applications and limitations, J. Electron. Packag. Trans. ASME 133 (2011) 041002-2.
[3] P.J. Marto, V.J. Lepere, Pool boiling heat transfer from enhanced surfaces to dielectric fluids, J. Heat Transfer – Trans. ASME 104 (1982) 292–299.
[4] W. Nakayama, T. Nakajima, S. Hirasawa, Heat sink studs having enhanced boiling surfaces for cooling of microelectronic components, ASME Paper 84-WA/HT-89, 1984.
[5] T.M. Anderson, I. Mudawar, Microelectronic cooling by enhanced pool boiling of a dielectric fluorocarbon liquid, J. Heat Transfer – Trans. ASME 111 (1989) 752–759.
[6] T.N. Tran, M.W. Wambsganss, D.M. France, Small circular- and rectangular-channel boiling with two refrigerants, Int. J. Multiphase Flow 22 (1996) 485–498.
[7] H.J. Lee, S.Y. Lee, Heat transfer correlation for boiling flows in small rectangular horizontal channels with low aspect ratios, Int. J. Multiphase Flow 27 (2001) 2043–2062.
[8] Y. Katto, M. Kunihiro, Study of the mechanism of burn-out in boiling system of high burn-out heat flux, Bull. JSME 16 (1973) 1357–1366.
[9] M. Monde, T. Inoue, Critical heat flux in saturated forced convective boiling on a heated disk with multiple impinging jets, J. Heat Transfer – Trans. ASME 113 (1991) 722–727.
[10] D.C. Wadsworth, I. Mudawar, Enhancement of single-phase heat transfer and critical heat flux from an ultra-high-flux-source to a rectangular impinging jet of dielectric liquid, J. Heat Transfer – Trans. ASME 114 (1992) 764–768.
[11] M.E. Johns, I. Mudawar, An ultra-high power two-phase jet-impingement avionic clamshell module, J. Electron. Packag. – Trans. ASME 118 (1996) 264–270.
[12] M.K. Sung, I. Mudawar, Experimental and numerical investigation of single-phase heat transfer using a hybrid jet-impingement/micro-channel cooling scheme, Int. J. Heat Mass Transfer 49 (2006) 682–694.
[13] M.K. Sung, I. Mudawar, Correlation of critical heat flux in hybrid jet impingement/micro-channel cooling scheme, Int. J. Heat Mass Transfer 49 (2006) 2663–2672.
[14] L. Lin, R. Ponnappan, Heat transfer characteristics of spray cooling in a closed loop, Int. J. Heat Mass Transfer 46 (2003) 3737–3746.
[15] M. Visaria, I. Mudawar, Theoretical and experimental study of the effects of spray orientation on two-phase spray cooling and critical heat flux, Int. J. Heat Mass Transfer 51 (2008) 2398–2410.
[16] I. Mudawar, M.A. El-Masri, C.S. Wu, J.R. Ausman-Mudawar, Boiling heat transfer and critical heat flux in high-speed rotating liquid films, Int. J. Heat Mass Transfer 28 (1985) 795–806.
[17] J.C. Sturgis, I. Mudawar, Assessment of CHF enhancement mechanisms in a curved, rectangular channel subjected to concave heating, J. Heat Transfer – Trans. ASME 121 (1999) 394–404.
[18] A.P. Ornatskii, L.S. Vinyarskii, Heat transfer crisis in a forced flow of underheated water in small-bore tubes, Teplofizika Vysokikh Temp. 3 (1965) 444–451.
[19] D.D. Hall, I. Mudawar, Ultra-high critical heat flux (CHF) for subcooled water flow boiling – II. High-CHF database and design parameters, Int. J. Heat Mass Transfer 42 (1999) 1429–1456.
[20] P.E. Jimenez, I. Mudawar, A multi-kilowatt immersion-cooled standard electronic clamshell module for future aircraft avionics, J. Electron. Packag. – Trans. ASME 116 (1994) 220–229.
[21] T.J. LaClair, I. Mudawar, Thermal transients in a capillary evaporator prior to the initiation of boiling, Int. J. Heat Mass Transfer 43 (2000) 3937–3952.
[22] I. Mudawar, D. Bharathan, K. Kelly, S. Narumanchi, Two-phase spray cooling of hybrid vehicle electronics, IEEE Trans. – Compon. Packag. Manufact. Tech. 32 (2009) 501–512.
[23] I. Mudawar, Micro-channel heat exchangers for metal hydride hydrogen storage systems, US Provisional Patent Application No. 61/184,595, 2009.
[24] M.B. Bowers, I. Mudawar, High flux boiling in low flow rate, low pressure drop mini-channel and micro-channel heat sinks, Int. J. Heat Mass Transfer 37 (1994) 321–332.
[25] W. Qu, I. Mudawar, Measurement and prediction of pressure drop in two-phase micro-channel heat sinks, Int. J. Heat Mass Transfer 46 (2003) 2737–2753.
[26] Y. Gan, J. Xu, S. Wang, Are the available boiling heat transfer coefficients suitable for silicon microchannel heat sinks?, Microfluids Nanofluids 4 (2008) 575–587
[27] H.Y. Wu, P. Cheng, Boiling instability in parallel silicon microchannels at different heat flux, Int. J. Heat Mass Transfer 47 (2004) 3631–3641.
[28] G. Wang, P. Cheng, A.E. Bergles, Effects of inlet/outlet configurations on flow boiling instability in parallel microchannels, Int. J. Heat Mass Transfer 51 (2008) 2267–2281.
[29] L. Jiang, M. Wong, Y. Zohar, Phase change in microchannel heat sinks with integrated temperature sensors, J. Microelectromech. Syst. 8 (1999) 358–365.
[30] S.M. Kim, J. Kim, I. Mudawar, Flow condensation in parallel micro-channels – Part 1: Experimental results and assessment of pressure drop correlations, Int. J. Heat Mass Transfer 55 (2012) 971–983.
[31] S.M. Kim, I. Mudawar, Flow condensation in parallel micro-channels – Part 2: Heat transfer results and correlation technique, Int. J. Heat Mass Transfer 55 (2012) 984–994.
[32] J. Lee, I. Mudawar, Fluid flow and heat transfer characteristics of low temperature two-phase micro-channel heat sinks. – Part 1: Experimental methods and flow visualization results, Int. J. Heat Mass Transfer 51 (2008) 4315–4326.
[33] W. Qu, I. Mudawar, S.-Y. Lee, S.T. Wereley, Experimental and computational investigation of flow development and pressure drop in a rectangular micro-channel, J. Electron. Packag. – Trans. ASME 128 (2006) 1–9.
[34] H. Lee, I. Park, I. Mudawar, M.M. Hasan, Micro-channel evaporator for space applications – 1. Experimental pressure drop and heat transfer results for different orientations in earth gravity, Int. J. Heat Mass Transfer (submitted for publication).
[35] M.K. Dobson, J.C. Chato, D.K. Hinde, S.P. Wang, Experimental evaluation of internal condensation of refrigerants R-134a and R-12, University of Illinois at Urbana-Champaign, ACRC TR-38, 1993.
[36] M.K. Dobson, J.C. Chato, S.P. Wang, D.K. Hinde, J.A. Gaibel, Initial condensation comparison of R-22 with R-134a and R-32/R-125, University of Illinois at Urbana-Champaign, ACRC TR-41, 1993.
[37] M.K. Dobson, J.C. Chato, J.P. Wattelet, J.A. Gaibel, M. Ponchner, P.J. Kenney, R.L. Shimon, T.c. Villaneuva, N.L. Rhines, K.A. Sweeney, D.G. Allen, T.T.

Hershberger, Heat transfer and flow regimes during condensation in horizontal tubes, University of Illinois at Urbana-Champaign, ACRC TR-57, 1994.
[38] H. Hirofumi, R.L. Webb, Condensation in extruded aluminum tubes, Penn State Research Report, Showa Aluminum Corporation, 1995.
[39] M. Zhang, A new equivalent Reynolds number model for vapor shear-controlled condensation inside smooth and micro-fin tubes (Ph.D. thesis), Pennsylvania State University, PA, 1998.
[40] W.W. Wang, Condensation and single-phase heat transfer coefficient and flow regime visualization in microchannel tubes for HFC-134a (MS thesis), Ohio State University, OH, 1999.
[41] Y.Y. Yan, T.F. Lin, Condensation heat transfer and pressure drop of refrigerant R-134a in a small pipe, Int. J. Heat Mass Transfer 42 (1999) 697–708.
[42] J.R. Baird, D.F. Fletcher, B.S. Haynes, Local condensation heat transfer rates in fine passages, Int. J. Heat Mass Transfer 46 (2003) 4453–4466.
[43] N.H. Kim, J.P. Cho, J.O. Kim, B. Youn, Condensation heat transfer of R-22 and R-410A in flat aluminum multi-channel tubes with or without micro-fins, Int. J. Refrig. 26 (2003) 830–839.
[44] J. Jang, P.S. Hrnjak, Condensation of CO2 at low temperature, University of Illinois at Urbana-Champaign, ACRC CR-56, 2004.
[45] A. Cavallini, D.D. Col, L. Doretti, M. Matkovic, L. Rossetto, C. Zilio, Condensation heat transfer and pressure gradient inside multiport minichannels, Heat Transfer Eng. 26 (2005) 45–55.
[46] B. Mitra, Supercritical gas cooling and condensation of refrigerant R410A at near-critical pressures (Ph.D. thesis), Georgia Institute of Technology, GA, 2005.
[47] J.S. Shin, M.H. Kim, An experimental study of flow condensation heat transfer inside circular and rectangular mini-channels, Heat Transfer Eng. 26 (2005) 36–44.
[48] U.C. Andresen, Supercritical gas cooling and near-critical-pressure condensation of refrigerant blends in microchannels (Ph.D. thesis), Georgia Institute of Technology, GA, 2006.
[49] T.M. Bandhauer, A. Agarwal, S. Garimella, Measurement and modeling of condensation heat transfer coefficients in circular microchannels, J. Heat Transfer – Trans. ASME 128 (2006) 1050–1059.
[50] O. Agra, I. Teke, Experimental investigation of condensation of hydrocarbon refrigerants (R600a) in a horizontal smooth tube, Int. Commun. Heat Mass Transfer 35 (2008) 1165–1171.
[51] Y.J. Kim, J. Jang, P.S. Hrnjak, M.S. Kim, Condensation heat transfer of carbon dioxide inside horizontal smooth and microfin tubes at low temperatures, J. Heat Transfer – Trans. ASME 131 (2009) 021501.
[52] K.A. Marak, Condensation heat transfer and pressure drop for methane and binary methane fluids in small channels (Ph.D. thesis), Norwegian University of Science and Technology, Trondheim, 2009.
[53] M. Matkovic, A. Cavallini, D.D. Col, L. Rossetto, Experimental study on condensation heat transfer inside a single circular minichannel, Int. J. Heat Mass Transfer 52 (2009) 2311–2323.
[54] C.Y. Park, P.S. Hrnjak, CO_2 flow condensation heat transfer and pressure drop in multi-port microchannels at low temperatures, Int. J. Refrig. 32 (2009) 1129–1139.
[55] A. Agarwal, T.M. Bandhauer, S. Garimella, Measurement and modeling of condensation heat transfer in non-circular microchannels, Int. J. Refrig. 33 (2010) 1169–1179.
[56] S. Bortolin, Two-phase heat transfer inside minichannels (Ph.D. thesis), University of Padua, Italy, 2010.
[57] D. Del Col, D. Torresin, A. Cavallini, Heat transfer and pressure drop during condensation of the low GWP refrigerant R1234yf, Int. J. Refrig. 33 (2010) 1307–1318.
[58] X. Huang, G. Ding, H. Hu, Y. Zhu, H. Peng, Y. Gao, B. Deng, Influence of oil on flow condensation heat transfer of R410A inside 4.18 mm and 1.6 mm inner diameter horizontal smooth tubes, Int. J. Refrig. 33 (2010) 158–169.
[59] H.K. Oh, C.H. Son, Condensation heat transfer characteristics of R-22, R-134a, R-410A in a single circular microtube, Exp. Therm. Fluid Sci. 35 (2011) 706–716.
[60] J.E. Park, F. Vakili-Farahani, L. Consolini, J.R. Thome, Experimental study on condensation heat transfer in vertical minichannels for new refrigerant R1234ze(E) versus R134a and R236fa, Exp. Therm. Fluid Sci. 35 (2011) 442–454.
[61] M. Derby, H.J. Lee, Y. Peles, M.K. Jensen, Condensation heat transfer in square, triangular, and semi-circular mini-channels, Int. J. Heat Mass Transfer 55 (2012) 187–197.
[62] K.M. Becker, Burnout measurements in vertical round tubes, effect of diameter, AE-TPM-RL-1260, Aktiebolaget Atomenergi, 1970.
[63] A.M. Lezzi, A. Niro, G.P. Beretta, Experimental data on CHF for forced convection water boiling in long horizontal capillary tubes, in: Proc. 10th Int. Heat Transfer Conf., UK, vol. 7, 1994, pp. 491–496.
[64] W.P. Baek, S.H. Chang, KAIST CHF data, Personal communication, Korea Advanced Institute of Science and Technology, Taejon, South Korea, December 8, 1997.
[65] G.M. Roach Jr., S.I. Abdel-Kahlik, S.M. Ghiaasiaan, M.F. Dowling, S.M. Jeter, Low-flow critical heat flux in heated microchannels, Nucl. Sci. Eng. 131 (1999) 411–425.
[66] H.C. Kim, W.P. Baek, S.H. Chang, Critical heat flux of water in vertical round tubes at low pressure and low flow conditions, Nucl. Eng. Des. 199 (2000) 49–73.
[67] Y. Yang, Y. Fujita, Boiling heat transfer in rectangular channels of small gaps, Mem. Fac. Eng. Kyushu Univ. 62 (2002) 223–239.
[68] W. Yu, D.M. France, M.W. Wambsganss, J.R. Hull, Two-phase pressure drop, boiling heat transfer, and critical heat flux to water in a small-diameter horizontal tube, Int. J. Multiphase Flow 28 (2002) 927–941.
[69] S. Saitoh, H. Daiguji, E. Hihara, Effect of tube diameter on boiling heat transfer of R-134a in horizontal small-diameter tubes, Int. J. Heat Mass Transfer 48 (2005) 4973–4984.
[70] R. Yun, Y. Kim, M.S. Kim, Convective boiling heat transfer characteristics of CO_2 in microchannels, Int. J. Heat Mass Transfer 48 (2005) 235–242.
[71] E. Hihara, C. Dang, Boiling heat transfer of carbon dioxide in horizontal tubes, in: Proc. 2007 ASME-JSME Thermal Eng. Summer Heat Transfer Conf., Canada, HT2007-32885, 2007, pp. 843–849.
[72] A. Greco, Convective boiling of pure and mixed refrigerants: an experimental study of the major parameters affecting heat transfer, Int. J. Heat Mass Transfer 51 (2008) 896–909.
[73] D. Shiferaw, Two-phase flow boiling in small- to micro-diameter tubes (Ph.D. thesis), Brunel University, UK, 2008.
[74] H. Ohta, K. Inoue, M. Ando, K. Watanabe, Experimental investigation on observed scattering in heat transfer characteristics for flow boiling in a small diameter tube, Heat Transfer Eng. 30 (2009) 19–27.
[75] L. Wang, M. Chen, M. Groll, Flow boiling heat transfer characteristics of R134a in a horizontal mini tube, J. Chem. Eng. Data 54 (2009) 2638–2645.
[76] C. Martín-Callizo, Flow boiling heat transfer in single vertical channel of small diameter (Ph.D. thesis), Royal Institute of Technology, Sweden, 2010.
[77] R. Ali, B. Palm, Dryout characteristics during flow boiling of R134a in vertical circular minichannels, Int. J. Heat Mass Transfer 54 (2011) 2434–2445.
[78] M. Ducoulombier, S. Colasson, J. Bonjour, P. Haberschill, Carbon dioxide flow boiling in a single microchannel – Part II: Heat transfer, Exp. Therm. Fluid Sci. 35 (2011) 597–611.
[79] H.K. Oh, C.H. Son, Evaporation flow pattern and heat transfer of R-22 and R-134a in small diameter tubes, Heat Mass Transfer 47 (2011) 703–717.
[80] H.K. Oh, C.H. Son, Flow boiling heat transfer and pressure drop characteristics of CO_2 in horizontal tube of 4.57-mm inner diameter, Appl. Therm. Eng. 31 (2011) 163–172.
[81] J.T. Oh, A.S. Pamitran, K.I. Choi, P. Hrnjak, Experimental investigation on two-phase flow boiling heat transfer of five refrigerants in horizontal small tubes of 0.5, 1.5 and 3.0 mm inner diameters, Int. J. Heat Mass Transfer 54 (2011) 2080–2088.
[82] J. Wu, T. Koettig, Ch. Franke, D. Helmer, T. Eisel, F. Haug, J. Bremer, Investigation of heat transfer and pressure drop of CO_2 two-phase flow in a horizontal minichannel, Int. J. Heat Mass Transfer 54 (2011) 2154–2162.
[83] D. Del Col, S. Bortolin, Investigation of dryout during flow boiling in a single microchannel under non-uniform axial heat flux, Int. J. Therm. Sci. 57 (2012) 25–36.
[84] T.G. Karayiannis, M.M. Mahmoud, D.B.R. Kenning, A study of discrepancies in flow boiling results in small to microdiameter metallic tubes, Exp. Therm. Fluid Sci. 36 (2012) 126–142.
[85] M. Li, C. Dang, E. Hihara, Flow boiling heat transfer of HFO1234yf and R32 refrigerant mixtures in a smooth horizontal tube: Part I. Experimental investigation, Int. J. Heat Mass Transfer 55 (2012) 3437–3446.
[86] R. Mastrullo, A.W. Mauro, J.R. Thome, D. Toto, G.P. Vanoli, Flow pattern maps for convective boiling of CO_2 and R410A in a horizontal smooth tube: experiments and new correlations analyzing the effect of the reduced pressure, Int. J. Heat Mass Transfer 55 (2012) 1519–1528.
[87] C.B. Tibiriçá, G. Ribatski, J.R. Thome, Flow boiling characteristics for R1234ze(E) in 1.0 and 2.2 mm circular channels, J. Heat Transfer – Trans. ASME 134 (2012) 020906.
[88] M.W. Wambsganss, D.M. France, J.A. Jendrzejczyk, T.N. Tran, Boiling heat transfer in a horizontal small-diameter tube, J. Heat Transfer – Trans. ASME 115 (1993) 963–972.
[89] T.N. Tran, Pressure drop and heat transfer study of two-phase flow in small channels (Ph.D. thesis), Texas Tech University, TX, 1998.
[90] C.C. Wang, C.S. Chiang, J.G. Yu, An experimental study of in-tube evaporation of R-22 inside a 6.5-mm smooth tube, Int. J. Heat Fluid Flow 19 (1998) 259–269.
[91] Y.Y. Yan, T.F. Lin, Evaporation heat transfer and pressure drop of refrigerant R-134a in a small pipe, Int. J. Heat Mass Transfer 41 (1998) 4183–4194.
[92] Z.Y. Bao, D.F. Fletcher, B.S. Haynes, Flow boiling heat transfer of Freon R11 and HCFC123 in narrow passages, Int. J. Heat Mass Transfer 43 (2000) 3347–3358.
[93] W. Qu, I. Mudawar, Flow boiling heat transfer in two-phase micro-channel heat sinks – I. Experimental investigation and assessment of correlation methods, Int. J. Heat Mass Transfer 46 (2003) 2755–2771.
[94] B. Sumith, F. Kaminaga, K. Matsumura, Saturated flow boiling of water in a vertical small diameter tube, Exp. Therm. Fluid Sci. 27 (2003) 789–801.
[95] R. Yun, Y. Kim, M.S. Kim, Y. Choi, Boiling heat transfer and dryout phenomenon of CO_2 in a horizontal smooth tube, Int. J. Heat Mass Transfer 46 (2003) 2353–2361.
[96] X. Huo, L. Chen, Y.S. Tian, T.G. Karayiannis, Flow boiling and flow regimes in small diameter tubes, Appl. Therm. Eng. 24 (2004) 1225–1239.
[97] J. Lee, I. Mudawar, Two-phase flow in high-heat-flux micro-channel heat sink for refrigeration cooling applications: Part II – Heat transfer characteristics, Int. J. Heat Mass Transfer 48 (2005) 941–955.
[98] R. Muwanga, I. Hassan, A flow boiling heat transfer investigation of FC-72 in a microtube using liquid crystal thermography, J. Heat Transfer – Trans. ASME 129 (2007) 977–987.
[99] X. Zhao, P.K. Bansal, Flow boiling heat transfer characteristics of CO_2 at low temperatures, Int. J. Refrig. 30 (2007) 937–945.

[100] B. Agostini, J.R. Thome, M. Fabbri, B. Michel, D. Calmi, U. Kloter, High heat flux flow boiling in silicon multi-microchannels – Part I: Heat transfer characteristics of refrigerant R236fa, Int. J. Heat Mass Transfer 51 (2008) 5400–5414.
[101] L. Consolini, Convective boiling heat transfer in a single micro-channel (Ph.D. thesis), École Polytechnique Fédérale De Lausanne, Switzerland, 2008.
[102] S.S. Bertsch, E.A. Groll, S.V. Garimella, Effects of heat flux, mass flux, vapor quality, and saturation temperature on flow boiling heat transfer in microchannels, Int. J. Multiphase Flow 35 (2009) 142–154.
[103] S. In, S. Jeong, Flow boiling heat transfer characteristics of R123 and R134a in a micro-channel, Int. J. Multiphase Flow 35 (2009) 987–1000.
[104] R. Mastrullo, A.W. Mauro, A. Rosato, G.P. Vanoli, Carbon dioxide local heat transfer coefficients during flow boiling in a horizontal circular smooth tube, Int. J. Heat Mass Transfer 52 (2009) 4184–4194.
[105] M. Ducoulombier, Ébullition convective du dioxyde de carbone – étude expérimentale en micro-canal (Ph.D. thesis), Institut National des Sciences Appliquées (INSA) de Lyon, France, 2010.
[106] M. Hamdar, A. Zoughaib, D. Clodic, Flow boiling heat transfer and pressure drop of pure HFC-152a in a horizontal mini-channel, Int. J. Refrig. 33 (2010) 566–577.
[107] C.L. Ong, Macro-to-microchannel transition in two-phase flow and evaporation (Ph.D. thesis), École Polytechnique Fédérale De Lausanne, Switzerland, 2010.
[108] C.B. Tibiriçá, G. Ribatski, Flow boiling heat transfer of R134a and R245fa in a 2.3 mm tube, Int. J. Heat Mass Transfer 53 (2010) 2459–2468.
[109] R. Ali, B. Palm, M.H. Maqbool, Flow boiling heat transfer characteristics of a minichannel up to dryout condition, J. Heat Transfer – Trans. ASME 133 (2011) 081501.
[110] K.H. Bang, K.K. Kim, S.K. Lee, B.W. Lee, Pressure effect on flow boiling heat transfer of water in minichannels, Int. J. Therm. Sci. 50 (2011) 280–286.
[111] J.B. Copetti, M.H. Macagnan, F. Zinani, N.L.F. Kunsler, Flow boiling heat transfer and pressure drop of R-134a in a mini tube: an experimental investigation, Exp. Therm. Fluid Sci. 35 (2011) 636–644.
[112] M.M. Mahmoud, T.G. Karayiannis, D.B.R. Kenning, Surface effects in flow boiling of R134a in microtubes, Int. J. Heat Mass Transfer 54 (2011) 3334–3346.
[113] W.W. Akers, H.F. Rosson, Condensation inside a horizontal tube, Chem. Eng. Prog. Symp. 56 (1960) 145–149.
[114] A. Cavallini, R. Zecchin, A dimensionless correlation for heat transfer in forced convection condensation, Proc. fifth Int. Heat Transfer Conf., Tyoko, Japan, vol. 3, 1974, pp. 309–313.
[115] M.M. Shah, A general correlation for heat transfer during film condensation inside pipes, Int. J. Heat Mass Transfer 22 (1979) 547–556.
[116] H. Haraguchi, S. Koyama, T. Fujii, Condensation of refrigerants HCFC 22, HFC 134a and HCFC 123 in a horizontal smooth tube (2nd report), Trans. JSME (B) 60 (1994) 245–252.
[117] M.K. Dobson, J.C. Chato, Condensation in smooth horizontal tubes, J. Heat Transfer – Trans. ASME 120 (1998) 193–213.
[118] K.W. Moser, R.L. Webb, B. Na, A new equivalent Reynolds number model for condensation in smooth tubes, J. Heat Transfer – Trans. ASME 120 (1998) 410–417.
[119] W.W. Wang, T.D. Radcliff, R.N. Christensen, A condensation heat transfer correlation for millimeter-scale tubing with flow regime transition, Exp. Therm. Fluid Sci. 26 (2002) 473–485.
[120] S. Koyama, K. Kuwahara, K. Nakashita, K. Yamamoto, An experimental study on condensation of refrigerant R134a in a multi-port extruded tube, Int. J. Refrig. 24 (2003) 425–432.
[121] T. Bohdal, H. Charun, M. Sikora, Comparative investigations of the condensation of R134a and R404A refrigerants in pipe minichannels, Int. J. Heat Mass Transfer 54 (2011) 1963–1974.
[122] M.M. Shah, An improved and extended general correlation for heat transfer during condensation in plain tubes, HVAC& R Res. 15 (2009) 889–913.
[123] Z. Sun, CO_2 flow boiling heat transfer in horizontal tubes (Ph.D. thesis), Purdue University, West Lafayette, IN, 2001.
[124] S.H. Yoon, E.S. Cho, Y.W. Hwang, M.S. Kim, K. Min, Y. Kim, Characteristics of evaporative heat transfer and pressure drop of carbon dioxide and correlation development, Int. J. Refrig. 27 (2004) 111–119.
[125] L. Wojtan, T. Ursenbacher, J.R. Thome, Investigation of flow boiling in horizontal tubes: Part I – A new diabatic two-phase flow pattern map, Int. J. Heat Mass Transfer 48 (2005) 2955–2969.
[126] L. Cheng, G. Ribatski, L. Wojtan, J.R. Thome, New flow boiling heat transfer model and flow pattern map for carbon dioxide evaporating inside horizontal tubes, Int. J. Heat Mass Transfer 49 (2006) 4082–4094.
[127] D. Del Col, F. Fantini, L. Rossetto, Dryout quality in a minichannel flow boiling, XXV UIT National Heat Transfer Conf., Italy, 2007, pp. 18–20.
[128] L. Cheng, G. Ribatski, J.M. Quibén, J.R. Thome, New prediction methods for CO_2 evaporation inside tubes: Part I – A two-phase flow pattern map and a flow pattern based phenomenological model for two-phase flow frictional pressure drops, Int. J. Heat Mass Transfer 51 (2008) 111–124.
[129] S. Jeong, D. Park, Evaporative heat transfer of CO_2 in a smooth and a micro-grooved miniature channel tube, Heat Transfer Eng. 30 (2009) 582–589.
[130] M.M. Shah, Chart correlation for saturated boiling heat transfer: equations and further study, ASHRAE Trans. 88 (1982) 185–196.
[131] M.G. Cooper, Saturation nucleate pool boiling – a simple correlation I., Chem. Eng. Symp. Ser. 86 (1984) 785–793.
[132] K.E. Gungor, R.H.S. Winterton, A general correlation for flow boiling in tubes and annuli, Int. J. Heat Mass Transfer 29 (1986) 351–358.
[133] Z. Liu, R.H.S. Winterton, A general correlation for saturated and subcooled flow boiling in tubes and annuli, based on a nucleate pool boiling equation, Int. J. Heat Mass Transfer 34 (1991) 2759–2766.
[134] G.M. Lazarek, S.H. Black, Evaporative heat transfer, pressure drop and critical heat flux in a small vertical tube with R-113, Int. J. Heat Mass Transfer 25 (1982) 945–960.
[135] G.R. Warrier, V.K. Dhir, L.A. Momoda, Heat transfer and pressure drop in narrow rectangular channels, Exp. Therm. Fluid Sci. 26 (2002) 53–64.
[136] B. Agostini, A. Bontemps, Vertical flow boiling of refrigerant R134a in small channels, Int. J. Heat Fluid Flow 26 (2005) 296–306.
[137] S.S. Bertsch, E.A. Groll, S.V. Garimella, A composite heat transfer correlation for saturated flow boiling in small channels, Int. J. Heat Mass Transfer 52 (2009) 2110–2118.
[138] W. Li, Z. Wu, A general correlation for evaporative heat transfer in micro/mini-channels, Int. J. Heat Mass Transfer 53 (2010) 1778–1787.
[139] S.M. Kim, I. Mudawar, Review of databases, predictive methods for pressure drop in adiabatic, condensing and boiling mini/micro-channel flows, Int. J. Heat Mass Transfer 77 (2014) 74–97.
[140] S.M. Kim, I. Mudawar, Universal approach to predicting two-phase frictional pressure drop for adiabatic and condensing mini/micro-channel flows, Int. J. Heat Mass Transfer 55 (2012) 3246–3261.
[141] S.M. Kim, I. Mudawar, Universal approach to predicting two-phase frictional pressure drop for mini/micro-channel saturated flow boiling, Int. J. Heat Mass Transfer 58 (2013) 718–734.
[142] S.M. Kim, I. Mudawar, Universal approach to predicting heat transfer coefficient for condensing mini/micro-channel flows, Int. J. Heat Mass Transfer 56 (2013) 238–250.
[143] S.M. Kim, I. Mudawar, Universal approach to predicting saturated flow boiling heat transfer in mini/micro-channels – Part II. Two-phase heat transfer coefficient, Int. J. Heat Mass Transfer 64 (2013) 1239–1256.
[144] S.M. Kim, I. Mudawar, Universal approach to predicting saturated flow boiling heat transfer in mini/micro-channels – Part I. Dryout incipience quality, Int. J. Heat Mass Transfer 64 (2013) 1226–1238.
[145] D.D. Hall, I. Mudawar, Critical heat flux (CHF) for water flow in tubes – I. Compilation and assessment of world CHF data, Int. J. Heat Mass Transfer 43 (2000) 2573–2604.
[146] D.D. Hall, I. Mudawar, Critical heat flux (CHF) for water flow in tubes – II. Subcooled CHF correlations, Int. J. Heat Mass Transfer 43 (2000) 2605–2640.
[147] R.K. Shah, A.L. London, Laminar Flow Forced Convection in Ducts: A Source Book for Compact Heat Exchanger Analytical Data, Academic press, New York, 1978 (Supl 1).
[148] H.M. Soliman, The mist-annular transition during condensation and its influence on the heat transfer mechanism, Int. J. Multiphase Flow 12 (1986) 277–288.
[149] E.W. Lemmon, M.L. Huber, M.O. McLinden, Reference fluid thermodynamic and transport properties – REFPROP Version 8.0, NIST, MD, 2007.
[150] R.W. Lockhart, R.C. Martinelli, Proposed correlation of data for isothermal two-phase, two-component flow in pipes, Chem. Eng. Prog. 45 (1949) 39–48.
[151] D.P. Traviss, W.M. Rohsenow, A.B. Baron, Forced-convection condensation inside tubes: a heat transfer equation for condenser design, ASHRAE Trans. 79 (1973) 157–165.
[152] S.W. Churchill, R. Usagi, A general expression for the correlation of rates of transfer and other phenomena, AIChE J. 18 (1972) 1121–1128.
[153] H. Mori, S. Yoshida, K. Ohishi, Y. Kakimoto, Dryout quality and post-dryout heat transfer coefficient in horizontal evaporator tubes, in: Eur. Therm. Sci. Conf., Germany, 2000, pp. 839–844.
[154] V.E. Schrock, L.M. Grossman, Forced convection boiling in tubes, Nucl. Sci. Eng. 12 (1962) 474–481.
[155] J.A. Shmerler, I. Mudawar, Local heat transfer coefficient in wavy free-falling turbulent liquid films undergoing uniform sensible heating, Int. J. Heat Mass Transfer 31 (1988) 67–77.
[156] J.A. Shmerler, I. Mudawar, Local evaporative heat transfer coefficient in turbulent free-falling liquid films, Int. J. Heat Mass Transfer 31 (1988) 731–742.
[157] T.H. Lyu, I. Mudawar, Statistical investigation of the relationship between interfacial waviness and sensible heat transfer to a falling liquid film, Int. J. Heat Mass Transfer 34 (1991) 1451–1464.
[158] T.H. Lyu, I. Mudawar, Determination of wave-induced fluctuations of wall temperature and convective heat transfer coefficient in the heating of a turbulent falling liquid film, Int. J. Heat Mass Transfer 34 (1991) 2521–2534.
[159] I. Mudawar, R.A. Houpt, Mass and momentum transport in Falling liquid films laminarized at relatively high Reynolds numbers, Int. J. Heat Mass Transfer 36 (1993) 3437–3448.
[160] I. Mudawar, R.A. Houpt, Measurement of mass and momentum transport in wavy-laminar falling liquid films, Int. J. Heat Mass Transfer 36 (1993) 4151–4162.
[161] J.E. Koskie, I. Mudawar, W.G. Tiederman, Parallel-wire probes for measurement of thick liquid films, Int. J. Multiphase Flow 15 (1989) 521–530.